






ISSN: 2617-6548

URL: www.ijirss.com


Application of hybrid neural network structures for modeling and control of combustion process

Laura Yesmakhanova^{1*},  Waldemar Wójcik²,  Seitzhan Orynbayev³,  Lesbek Satayev⁴

^{1,3,4}Taraz University named after M.Kh.Dulaty, Taraz, Kazakhstan.

²Politechnika Lubelska Institute of Electronics and Information Technology, Lublin, Poland.

Corresponding author: Laura Yesmakhanova (Email: yesmakhanovalaura@gmail.com)

Abstract

The scientific work is based on the need to develop a combustion process control system that will optimize boiler operation based on information and measurements, as well as take into account innovative methods for assessing process quality. Modern methods of obtaining information about combustion quality (CO and NO_x emissions) in combination with control methods make it possible to reduce harmful gas emissions into the atmosphere and efficiently use fuel associated with renewable energy sources. The dynamics of the combustion process of coal dust and biomass are complex; therefore, three selected deep neural network structures were considered for the study: MLP, simple recurrent network, and LSTM (Long Short Term Memory) cells. The study proposes a new hybrid model based on data processing, which uses selected decomposition methods to divide the total parameters of the combustion process into sublayers. In this work, two MRAC systems were developed and compared. The study considered direct forecasting with a five-step horizon. According to the analysis results, the best results for modeling the time series of the combustion process were obtained using the hybrid EWT-LSTM-RELM-IEWT method. The results obtained on the laboratory bench made it possible to develop robust control using hybrid neural networks.

Keywords: Combustion process, Control, Diagnostics, Neural networks, NO_x emissions, Optical methods.

DOI: 10.53894/ijirss.v8i5.9194

Funding: This study received no specific financial support.

History: Received: 27 June 2025 / **Revised:** 30 July 2025 / **Accepted:** 1 August 2025 / **Published:** 8 August 2025

Copyright: © 2025 by the authors. This article is an open access article distributed under the terms and conditions of the Creative Commons Attribution (CC BY) license (<https://creativecommons.org/licenses/by/4.0/>).

Competing Interests: The authors declare that they have no competing interests.

Authors' Contributions: Concept development, statistical analysis, research experiment, project management, author coordination, Yesmakhanova Laura (YL). Study aim, methodology contribution, research methodology development, Waldemar Wójcik (WW). Statistical processing, result interpretation, Results and Discussion writing, Seitzhan Orynbayev (SO). Literature review, Introduction writing, article editing, Lesbek Satayev (LS). All authors have read and agreed to the published version of the manuscript.

Transparency: The authors confirm that the manuscript is an honest, accurate, and transparent account of the study; that no vital features of the study have been omitted; and that any discrepancies from the study as planned have been explained. This study followed all ethical practices during writing.

Publisher: Innovative Research Publishing

1. Introduction

Coal remains the primary fuel source in the energy sector. Due to its dwindling resources and the associated emissions of harmful combustion products, efforts are constantly being made to change this situation. To this end, a number of

technologies have been developed to improve combustion efficiency, such as: staged air cooling, reduction of NO_x emissions through afterburning, and flue gas recirculation systems. The afterburning method involves feeding fuel into the furnace in two combustion zones: the first, where the main fuel is burned, and the second, where the additional fuel is partially burned, creating a reducing atmosphere. This is particularly important in low-emission co-firing technologies for coal and biomass, where the cost of meeting emission requirements directly affects the stability (efficiency) of the combustion process and indirectly affects increased corrosion and slagging of the boiler. These undesirable effects can be limited by precise control using additional process information [1].

Among the available diagnostic methods, most are very expensive or simply impractical in industrial conditions. Optical and acoustic methods are an interesting alternative. In the first group, the radiation emitted by the flame (flame core) reflects changes associated with chemical and physical changes occurring during combustion. Therefore, it can be assumed that this approach provides additional, real-time (not delayed), and spatially selective diagnostic information about the combustion process. As a necessary condition for such a solution, it should be assumed that the stable and stationary position of the flame corresponds to a dynamic equilibrium that includes the local flame propagation velocity and the velocity of the incoming fuel mixture [1, 2]. This suggests that the shape of the flame can be an indicator of the combustion process occurring under specific conditions. As a result, there is a relationship between the parameters describing the changes in the flame and the temperature of the gases leaving the combustion chamber (boiler). Taking this information into account by the control system, in addition to the classic measurements of temperature changes and inertial characteristics, will ensure a quick and safe response from the controller.

The use of deep neural networks for clustering tasks and other areas of machine learning is quite common. An interesting alternative is the use of a recurrent variant of the LSTM (Long Short-Term Memory) network for identifying and controlling dynamic systems. LSTM is currently one of the most popular deep neural network structures. It can be used to effectively manage the memory of past (historical) states. The rationale for choosing this algorithm structure is deep learning networks. Arguments in favor of this solution include limiting the vanishing gradient problem and the potential for representing system dynamics.

In complex energy processes, the ability to accurately predict parameters is of great importance. The range of possible applications for different types of models is wide. They can be broadly divided into physical models, statistical models, heuristic models (usually using artificial intelligence methods), and hybrid models.

Models that utilize artificial intelligence methods can simulate nonlinearity. Due to the particularly unstable characteristics of the combustion process, using a single artificial intelligence model often results in the model becoming trapped in local minima. This prevents the model from achieving satisfactory performance in diagnostic and control tasks. Hybrid solutions are employed to address these limitations. Current trends indicate two main directions in the development of hybrid models. One approach involves combining multiple predictors, where their prediction results are integrated to produce the final prediction. Examples include FFBPNN (forward propagation neural network), BPNN (backward propagation neural network), and BFGSNN (Broyden Fletcher Goldfarb Shannon neural network), which serve as predictors, with their results combined using GP (genetic programming) methods. The other approach focuses on data processing, where selected decomposition methods are used to divide the summary parameters of the combustion process into sublayers. Each sublayer is then predicted by its own predictor, and the resulting data enables the reconstruction of the final prediction. The decomposition of the output information signal is a crucial element in the development of a hybrid model.

The paper proposes a new hybrid model, which is constructed as follows:

- EWT is used to decompose the original measurement series into several sublayers;
- An LSTM network is used to predict each sublayer;
- A RELM network is used to model the error series of each decomposed sublayer;
- IEWT is used for reconstruction to recreate the predicted sublayers and filter out outliers.

It is also possible to use a hybrid EWT model that decomposes the signal preprocessing and a postprocessing structure based on IEWT-EWT reconstruction as a relatively new signal processing method used for adaptive conversion of the original signals into several sublayers during preprocessing. Furthermore, IEWT is employed to rectify outliers during the post-processing phase. The proposed pre-processing and post-processing structure can be generalized to other signal processing algorithms, such as wavelet packet decomposition (WPD), variational mode decomposition (VMD), etc.

Furthermore, the employment of an LSTM network is a viable option, constituting one of the most prevalent deep learning methodologies for sequence analysis. The potential of the LSTM network will be analyzed as a single predictive model or as part of a hybrid in various algorithms combining architectures.

The study proposes a hybrid predictor based on error modeling. In the hybrid predictor, an LSTM (Long Short-Term Memory) network is used as the primary predictor, while a RELU (Rectified Linear Unit) network, a popular machine learning method, is used as an auxiliary predictor to model a series of prediction errors obtained from the built-in LSTM network. The error modeling method has heretofore been employed to enhance the performance of ARIMA, ELM, and LSSVM models; consequently, it is intriguing to assess the prediction outcomes of the LSTM network in conjunction with RELM. The combination of the LSTM network and the RELM network will be integrated with the EWT decomposition of the IEWT reconstruction structure.

In contrast to other hybrid forecasting methods based on deep learning, this approach considers not only the forecasting accuracy parameter but also the computational load inherent to the properties of LSTM.

In order to verify the effectiveness of the proposed solutions, a number of models were utilized to average the time series of selected measured parameter values. The effectiveness of the models was evaluated at varying forecasting intervals.

The procedure for constructing the EWT-LSTM-RELM-IEWT hybrid model is shown in Figure 1.

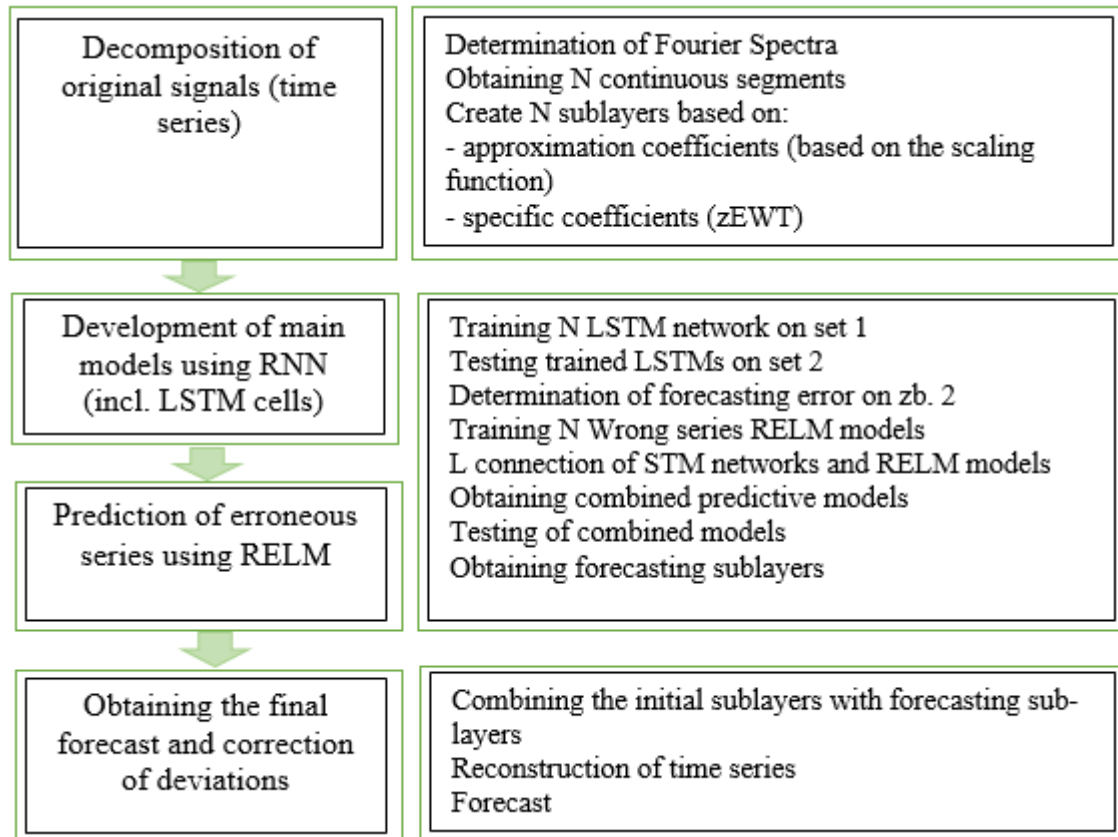


Figure 1.
Stages of creating a hybrid model.

Detailed descriptions are explained as follows:

1. The initial measurement data is decomposed into a series of sublayers using the EWT algorithm.
2. The sublayers are divided into two training sets. Each data set is used to construct input and output matrices in accordance with the multi-step forecasting method (Figure 2).

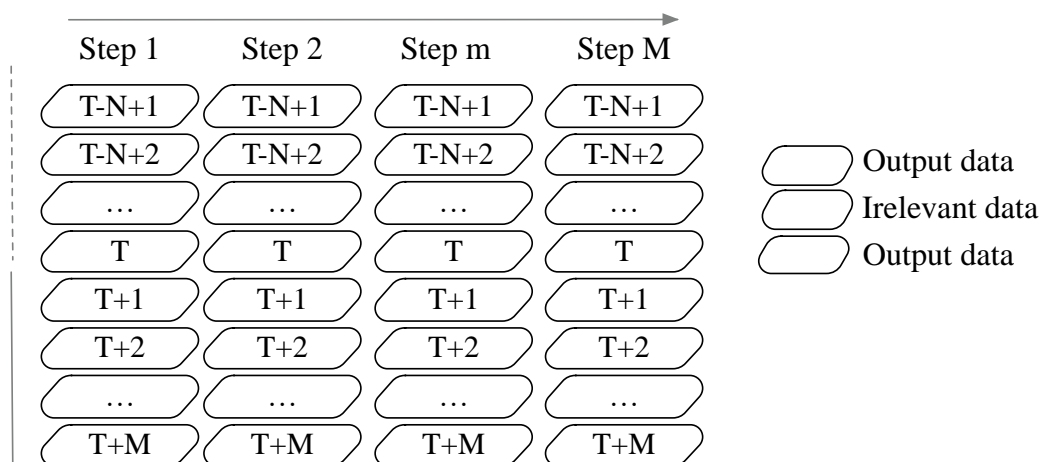


Figure 2.
The multi-year forecasting model used in the decision.

1. LSTM models are constructed based on the initial training set and are used to predict the decomposed series of input data. Subsequently, the models are evaluated using the second test set. The series of prediction error values for the second training set are determined by calculating the series predicted from the original subsets.

2. The RETM models are constructed based on a series of model error values from the second training set, with the purpose of predicting the prediction errors of LSTM models.

3. The LSTM and RELM models are then combined to create a unified prediction model, which is subsequently tested on a test set to obtain prediction results for each sublayer that has been previously defined.

4. The forecast data for each individual sublayer is then combined with the corresponding source sublayer. The subsequent utilization of Fourier spectrum segments from the source measurement data series facilitates the determination of bandpass filters. The IEWT algorithm is utilized for the reconstruction of composite sublayers and the subsequent acquisition of final forecast results.

5. The study examined direct forecasting with one-step and five-step horizons. To ascertain the efficacy of the proposed EWT-LSTM-RELM-IEWT hybrid model in wind speed forecasting, a total of seven distinct models were considered. The models employed in this study included a single backward propagation (BP) model, a single recurrent linear model (RELM), a single long short-term memory (LSTM) model, a hybrid long short-term memory-recurrent linear model (LSTM-RELM), a hybrid event-based language model-long short-term memory (EWT-LSTM), and a hybrid EWT-LSTM-recurrent linear model (EWT-LSTM-RELM).

In industrial practice, real-time assessment of the combustion process is critically important, given the typically very limited computing capabilities of industrial measurement and control systems. Consequently, such an evaluation should be conducted employing the minimum necessary number of diagnostic signals. The flame structure is characterized by heterogeneity; therefore, it is necessary to determine the area most sensitive to changes in the burner operating point. Each boiler type possesses distinct characteristics. It is imperative to note that boilers and burners vary in nature and function. Consequently, the optical system must undergo individual adaptation to ensure optimal performance and compatibility. The determination of certain parameters of the optical system is possible based on the boiler design. However, the optimization of the optical system necessitates testing on an operating installation [3]. In order to achieve this objective, an analysis of the optical signals from individual flame zones was conducted. The flame zone that exhibited the greatest sensitivity to alterations in burner input parameters was identified through the implementation of principal component analysis (PCA) on the corresponding signals. The present study provides an example of the procedure for one of the largest units built in Poland the AP-1650 boiler.

2. Research Methods

Tests on the combustion of coal dust and biomass were conducted on a test bench (Figure 9). A low-NO_x burner with a diameter of 0.1 m was installed horizontally on the front wall of the chamber. The bench had all the necessary fuel supply systems, including primary and secondary air, coal, and oil. Pre-prepared coal powder was stored in a hopper and fed by a feeder. In the case of biomass, coal dust was mixed with straw after passing through the feeder.

The combustion chamber is equipped with viewing apertures on both sides, facilitating observation of the combustion process and enabling the capture of images. During the testing phase, a high-speed camera equipped with a CMOS (Complementary Metal-Oxide-Semiconductor) sensor was strategically positioned in close proximity to the burner nozzle, as this specific area was deemed to be of paramount importance. The camera was capable of recording images with a resolution of 1280 x 1024 pixels at a rate of 500 frames per second. A 0.7 mm borescope was utilized to record images of the flame from within the combustion chamber. The optical system was cooled by a water jacket, and purified air was blown through the probe lenses to prevent contamination. This procedure, which is important for the process of recording, has been observed to cause minor interference in the combustion area in proximity to the burner [3].

The initiation of the test bench resembles the start of a power boiler. Initially, the test bench is preheated using hot air. Since the temperature is not sufficiently high for volatile substances to be released from the coal, only the auxiliary oil burner, ignited by a gas burner, is activated at the start of the test. It is important to note that when the temperature in the combustion chamber exceeds the auto-ignition temperature of coal (approximately 200°C), a screw coal feeder rotating at 1.5 s⁻¹ (90 rpm) is initiated. The coal dust introduced into the burner is ignited by the operating fuel oil burner. Once the temperature within the combustion chamber reaches a level suitable for the reliable ignition of pulverized coal fuel, the fuel oil burner is deactivated. Subsequently, the pulverized coal burner becomes the sole active component. The fuel feed rate is increased until the necessary experimental conditions are met. The solid fuel output is not directly proportional to the feed rate and is calculated based on the decrease in fuel mass from the hopper. The procedure for stopping the test rig involves burning the residual fuel within the hopper, in the presence of a fuel oil flame. After the complete removal of solid fuel from the hopper and dust pipes, the fuel oil burner is deactivated. The chamber is ventilated with secondary air until the temperature drops below the level that would allow the installation to be fully shut down [4].

Two types of fuel were subjected to testing: pure coal and a mixture of coal and biomass. The mixture was prepared prior to the combustion testing. The tests were conducted with biomass content in the mixture set at 10%, 20%, and 30% for two types of biomass: shredded straw and shredded wood chips. The experimental design encompassed the combustion of both fuel types at three levels of chamber heat load, in conjunction with three conditions of excess air. The excess air was selected so that one condition corresponded to normal combustion conditions in a low-emission swirl burner ($\lambda \approx 0.77$), and the other two cases corresponded to higher and lower values, respectively.

Table 1 presents the mean values of the primary test parameters. It is important to note that each test was recorded only after thermal equilibrium had been established within the chamber, with each test lasting for a period of 300 seconds. During the course of the experiment, the combustion conditions (fuel and air consumption, temperature, etc.) were maintained at constant levels [4]. The measurement method has been developed with the specific purpose of negating the potential impact of transport delays on gas analyzers. It is hypothesized that the conditions during the measurement are stationary and the emission values are stable. This is of significance due to the influence of negative pressure in the combustion chamber on the delay and the difficulty of obtaining the same negative pressure value for all measurements.

Furthermore, this strategy precludes the training of dynamic neural networks due to data gaps. The sampling frequency was set at 8192 Hz for each individual channel.

Table 1.

Key test parameters (average values).

Test number	Fuel	Secondary air flow	Fuel consumption	Excess air	Moc
1	coal	151.16	54.08	~0.65	400
2		185.95	54.61	~0.77	400
3		210.51	55.14	~0.85	400
4		93.03	41.55	~0.65	300
5		121.35	41.61	~0.77	300
6		148.51	41.98	~0.85	300
7		72.81	33.78	~0.65	250
8		96.35	33.93	~0.77	250
9		126.71	34.85	~0.85	250
10	coal + 10% biomass	128.75	56.76	~0.65	400
11		213.74	55.90	~0.77	400
12		129.06	53.43	~0.85	400
13		74.66	41.88	~0.65	300
14		104.60	42.75	~0.77	300
15		152.22	44.17	~0.85	300
16		64.89	37.02	~0.65	250
17		78.56	35.00	~0.77	250
18		109.58	34.21	~0.85	250

When combustion parameters are changed, the instantaneous intensity depends on the stoichiometry of combustion (Figure 3), thermal load (power) (Figure 4), and fuel type (Figure 5). Interpreting the raw oscillograms is quite challenging. To verify whether the combustion process is functioning correctly (diagnostics), it is necessary to further process the signals to obtain information that an operator can understand or utilize in the boiler control system.

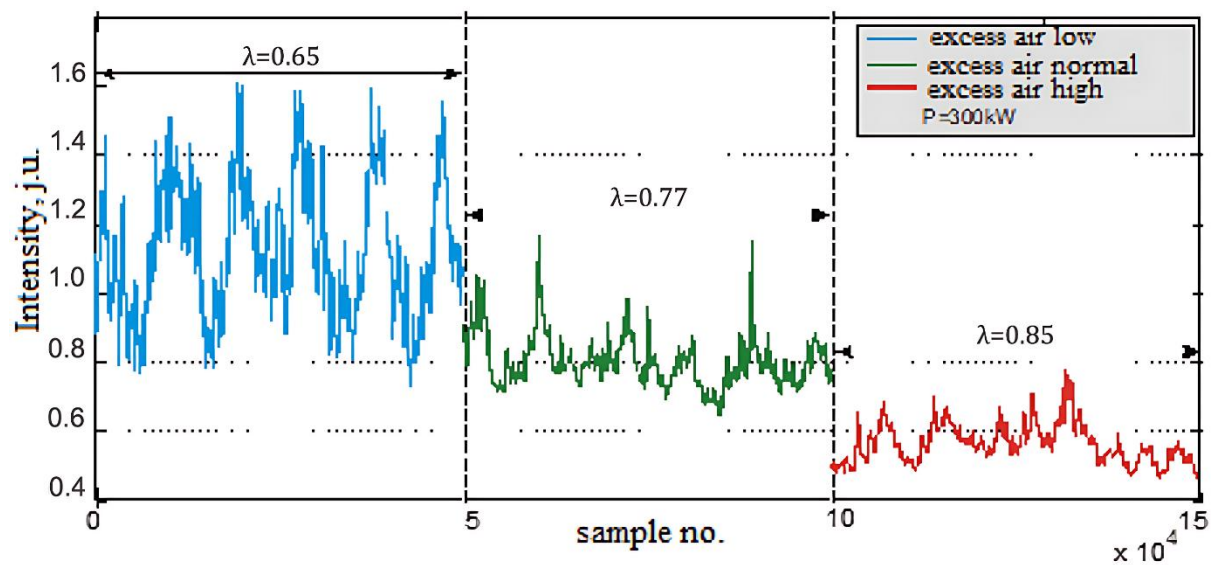


Figure 3.
Intensity dynamics at various air excess coefficients.

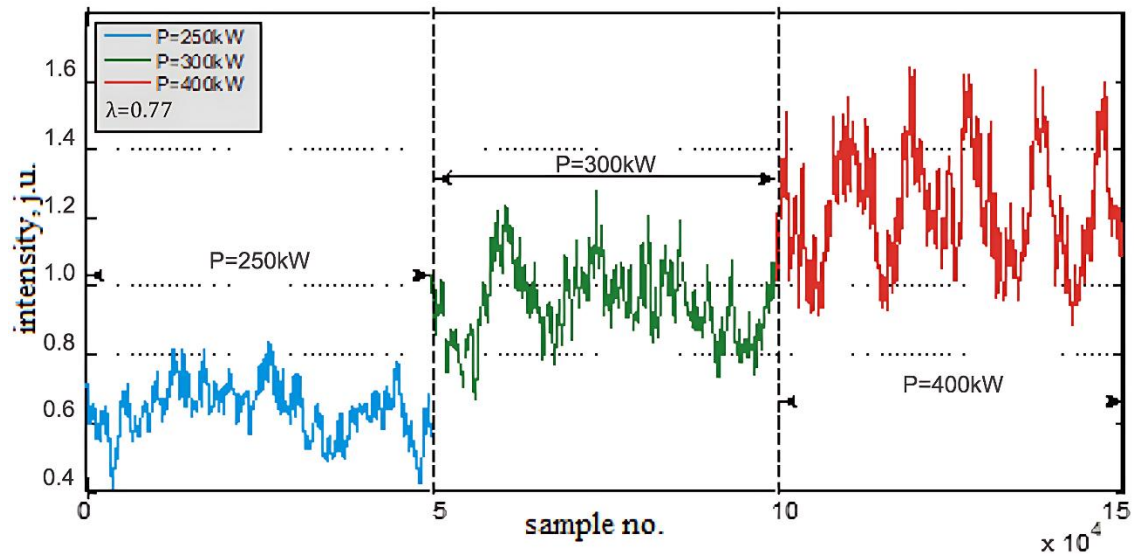


Figure 4.
Temporal dependencies of intensity for different powers.

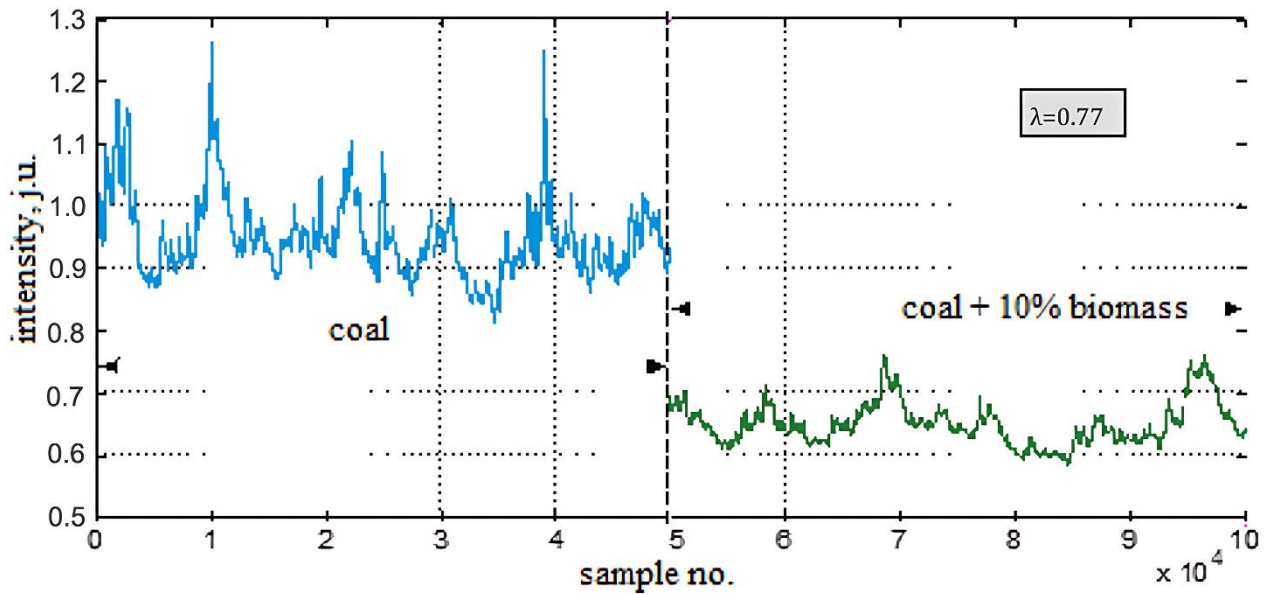


Figure 5.
Temporary changes in intensity for coal and coal-biomass mixtures.

Figure 6 shows a structural diagram of a boiler with a furnace, riser/evaporator, drum, steam superheater, cooler, and intermediate steam superheater with input and output parameters connected to the boiler unit's process circuits.

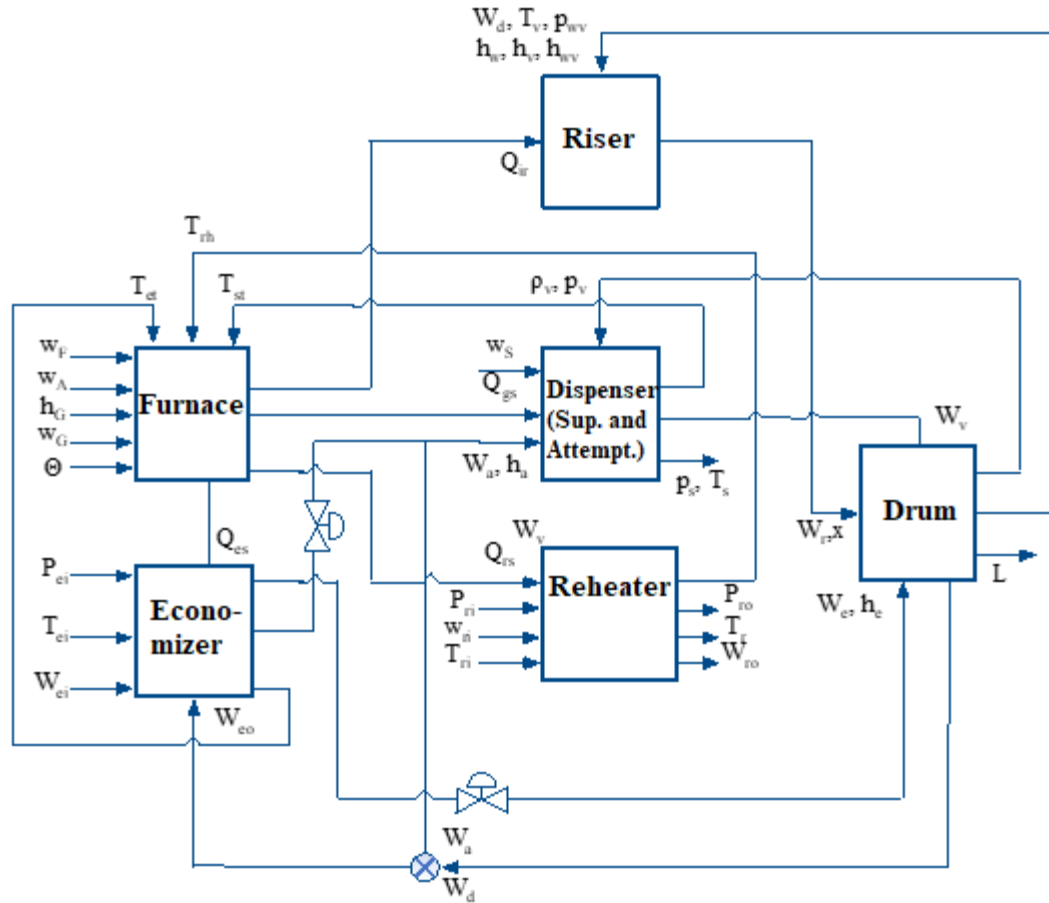


Figure 6.
Structural diagram of the combustion control system for a pulverized coal boiler.

The furnace, also known as the combustion chamber, supplies heat to the heat transfer system. Time, temperature, and turbulence are the three main parameters required for burning pulverized coal in a balanced draft boiler furnace.

Where:

- w_F - Fuel consumption in the furnace [kg/s],
- w_A - Air flow to the surface [kg/s],
- h_G - Enthalpy of steam turbine exhaust gases [J/kg],
- w_G - Exhaust gas flow from steam turbine [kg/s],
- θ - Slope coefficient $[0 < \theta < 1]$ rad,
- T_{st} - Temperature of metal elements of the steam superheater [K],
- T_{rh} - Temperature of metal elements of the heater (steam superheater) [K],
- T_{et} - Temperature of metal elements of the economizer [K],
- h_A - Enthalpy of incoming air [J/kg].

Parameters:

- k - gain coefficient,
- k_F - Coefficient of friction [m•s],
- K_{gs} - Experimental heat transfer coefficient to the steam superheater [J/(kg•K)],
- c_{gs} - Thermal efficiency of gas combustion [J•s/(kg•K)],
- k_{rs} - Experimental heat transfer coefficient to the heater [J/(kg•K)],
- V_F - Combustion chamber volume [m³],
- C_F - Calorific value of fuel [J/kg],
- R_S - Air-fuel ratio (lambda),
- γ - Fresh air content in steam turbine exhaust gases,
- k_{es} - Experimental heat transfer coefficient to the economizer [J/(kg•K)],
- ρ_{EG} - Boiler exhaust gas density [kg/m³].

Outputs:

- Q_{ir} - Heat transferred to risers [J/s],
- Q_{is} - Heat transferred by radiation to the steam superheater [J/s],
- Q_{rs} - Heat transferred to the heater (steam superheater) [J/s],
- Q_{es} - Heat transferred to the economizer [J/s],
- p_G - Air pressure in the boiler [Pa],

Q_{gs} - Total heat transferred to the steam superheater [J/s],
 h_{EG} - Enthalpy of exhaust gases from the boiler [J/s],
 w_{EG} - Mass flow rate of exhaust gases from the boiler [kg/s],
 T_g - Gas temperature in the steam superheater [K],
 T_{g1} - Exhaust gas temperature in the boiler [K],
 γ - Percentage of excess air [%].

Figure 7 shows a furnace model that considers the following equations, input signals, parameters, states, and output signals. Based on this, a general boiler control model was developed using MATLAB/Simulink software. The figure illustrates blocks representing individual subsystems of the coal-fired power plant model.

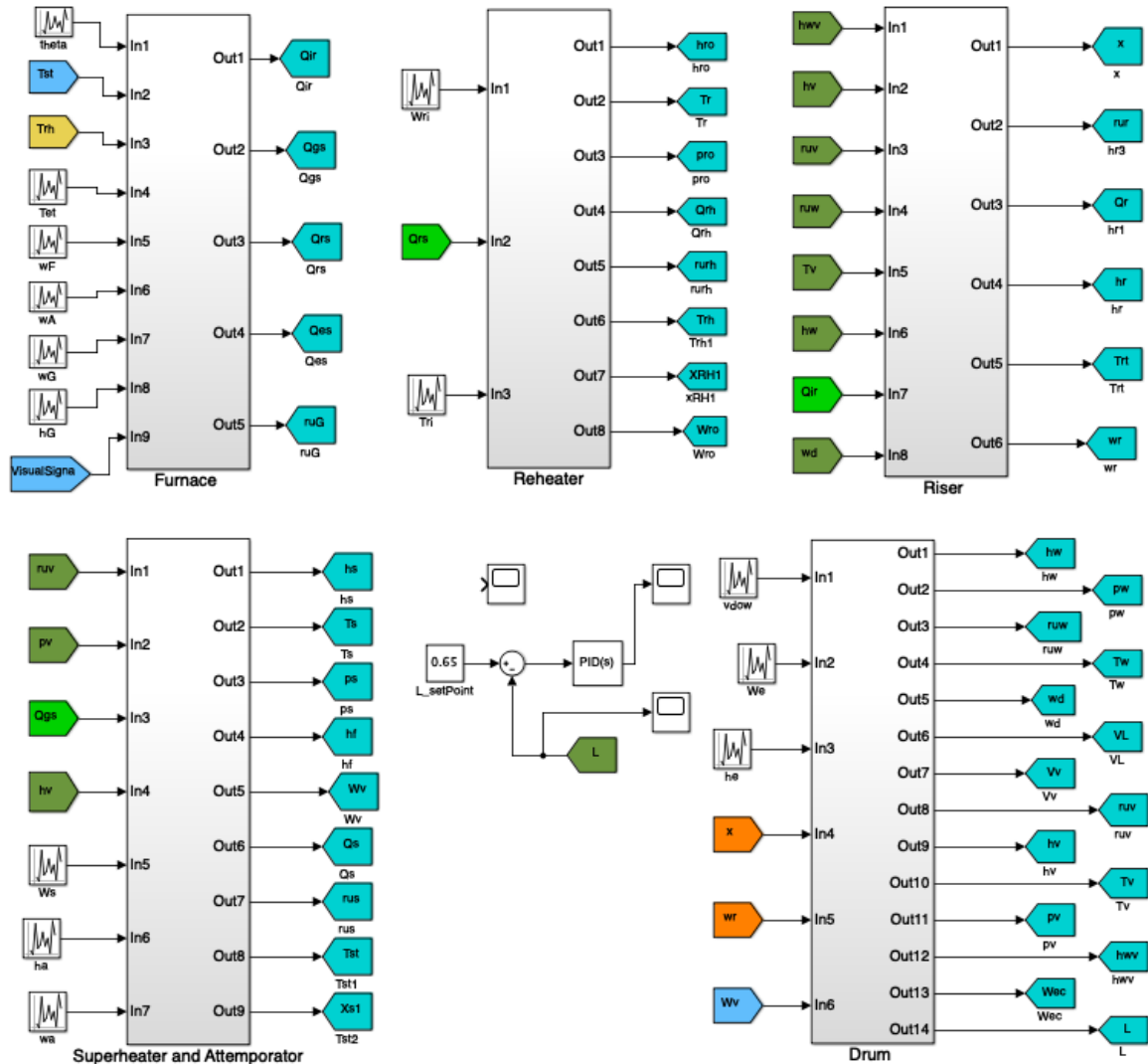


Figure 7.
 Integrated model of the combustion process at a coal-fired power plant in Simulink, MATLAB.

The development of individual subsystems was informed by mathematical equations and physical relationships that delineate the operational dynamics of boilers.

The furnace, also known as the combustion chamber, is the component that extracts energy from fuel in the form of heat. It serves as the starting point for the heat transfer system. The three fundamental parameters required for initiating combustion are time, temperature, and turbulence (i.e., swirl). Furthermore, it is essential to maintain negative pressure within the combustion chamber during boiler operation.

As illustrated in Figure 8, the developed combustion chamber model encompasses equations, input signals, parameters, states, and output signals.

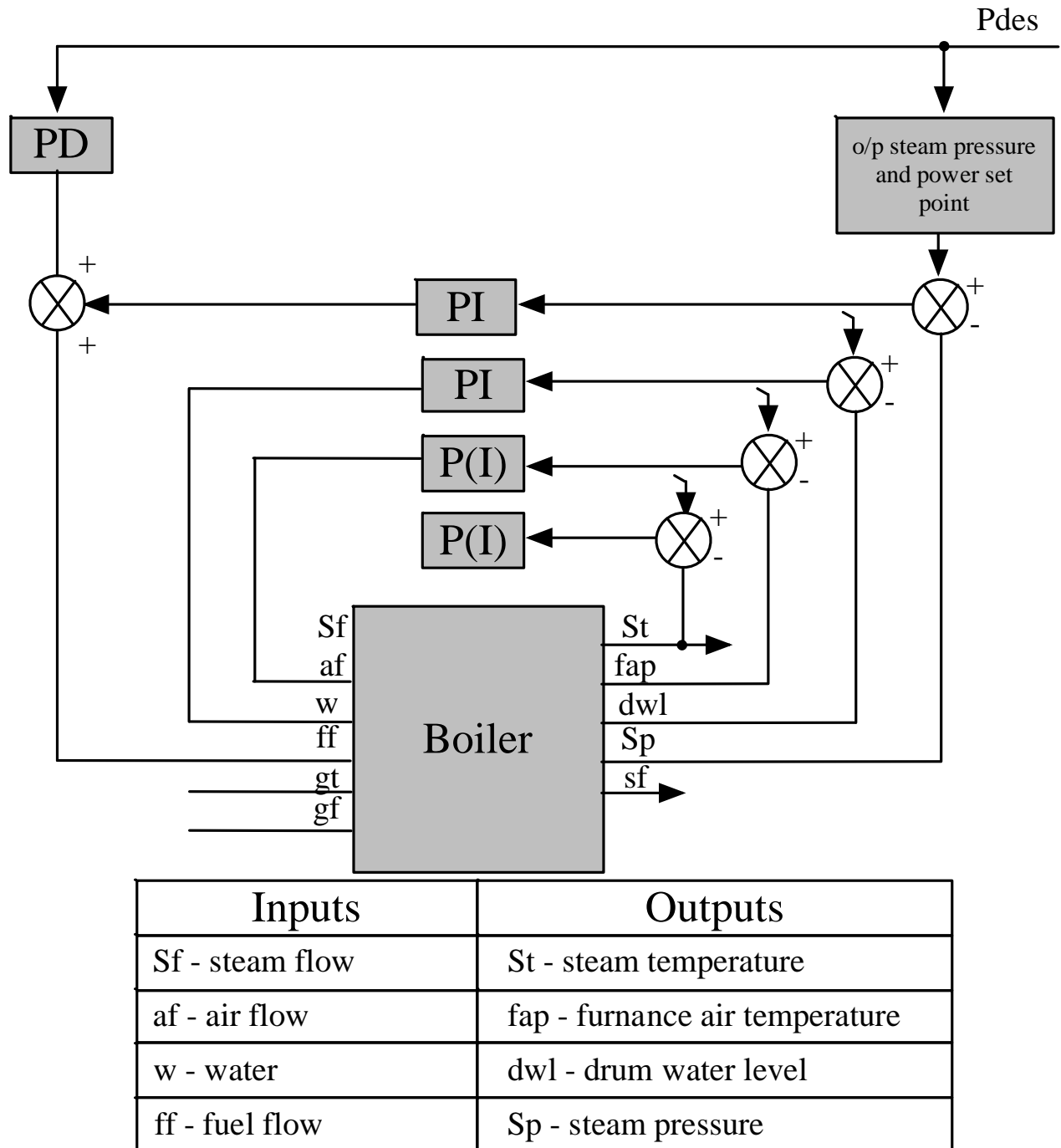


Figure 8.
Schematic diagram of local boiler control circuits and associated inputs and outputs.

The significant financial investment required for implementing secondary method solutions is a key factor that limits their affordability to a select group of energy producers.

In the energy sector, which primarily relies on the combustion of hard coal, lignite, and the co-combustion of biomass, significant emphasis is placed on primary methods. It is estimated that innovative technologies based on primary methods will enable compliance with emission limits (in accordance with the IPPC (Integrated Pollution Prevention and Control) and LCP (Large Combustion Plants) directives) at half the cost of catalytic reduction methods.

The significant environmental impact is counterbalanced by the financial implications, in addition to the challenges and delays associated with acquiring permits, even for novel investments. The pivotal concern in this scenario pertains to the cost-effective mitigation of nitrogen oxide (NO_x) emissions.

It is evident that, due to the inherent complexity and non-linearity of the combustion process, delays and failures are inevitable. Furthermore, safety issues are also a pertinent concern. Consequently, the majority of the discussed and implemented solutions are primarily focused on modernization. The principal measures available to developers of low-emission combustion systems are confined to the following: reducing the combustion temperature, air distribution, staged fuel supply (combustion aerodynamics and afterburning), and considering the reducing properties of a rich flame [5].

In existing facilities, modernization is achieved through the implementation of advanced technologies, incorporating state-of-the-art low-emission burners and staged air supply systems in OFA configurations. Technologies that facilitate process control can be regarded as either an alternative or a supplement to these technological improvements [2].

Low-emission burners for pulverized fuel utilize the reducing properties of a rich pulverized flame, forming zones of stoichiometric combustion through staged air or fuel supply. However, the staging of air or fuel supply in pulverized burners has been demonstrated to compromise combustion stability and increase unburned fuel.

The continuous measurement of dust flow in dust ducts is a challenging endeavor; however, it provides valuable information regarding the input parameters of the process. Furthermore, at the culmination of the process, acquiring real-time data related to the combustible composition of ash, notably the organic carbon content, is of paramount importance [6].

The acquisition of such information necessitates two distinct competencies. Firstly, it requires the capacity to undertake measurements at a genuine facility. Secondly, it necessitates the utilization of sophisticated measuring equipment, which is often costly.

The experimental tests were conducted on a 0.5 MW test bench using a pulverized coal burner. The configuration of the test bench for the co-combustion process is illustrated in Figure 9.

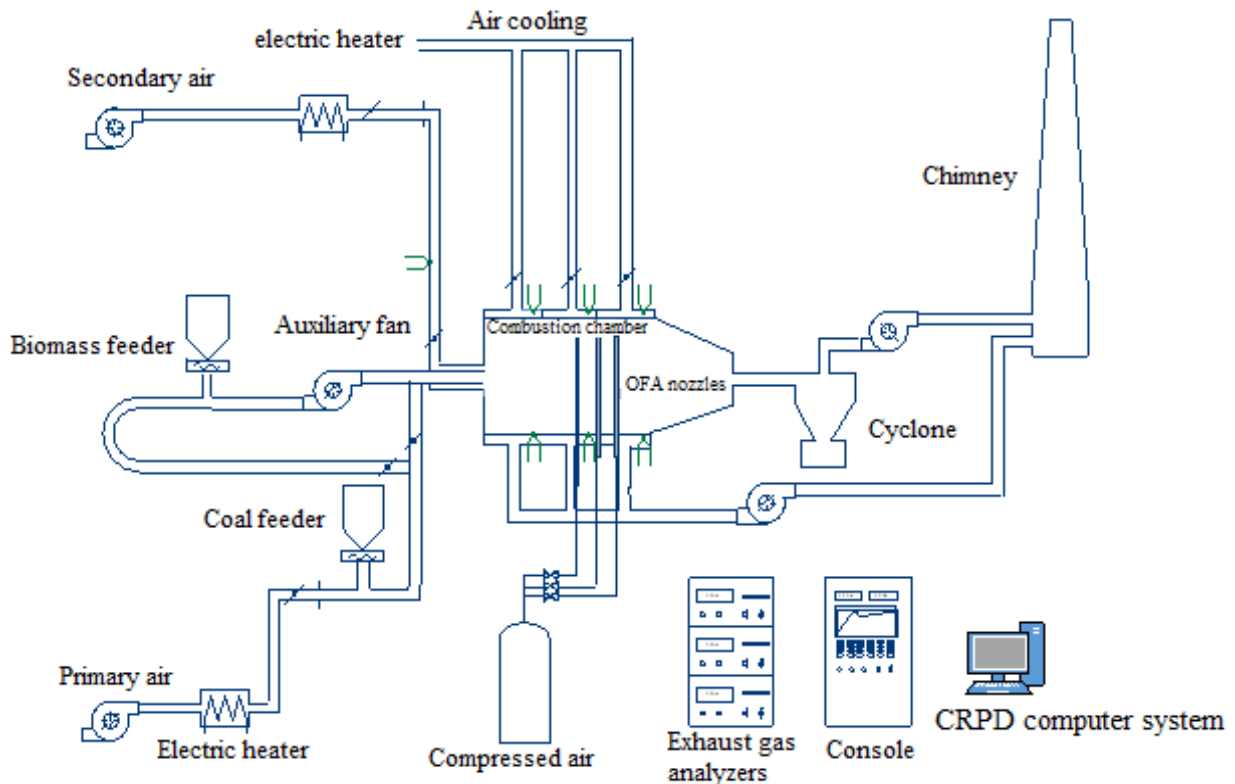


Figure 9.
Schematic diagram of a stand for testing the combustion process.

The primary component of the test bench is a cylindrical combustion chamber, the interior of which is lined with heat-insulating material, while the exterior is air-cooled. The front wall of the combustion chamber is cooled by water. A pulverized coal burner has been installed along the axis of the front wall. An auxiliary fuel oil burner is utilized for the purpose of heating the test bench and igniting the pulverized coal fuel. The installation of the device is undertaken along the axis of the pulverized coal burner or in the front panel, with the specific location determined by the design parameters of the burner. The primary air flow rate to the burner is 250 m³/h, and the secondary air flow rate is up to 500 m³/h [3, 7].

The prepared pulverized fuel, consisting of ground coal and biomass or a mixture thereof, is fed into the fuel bunker, from where the feeder supplies it to the primary air duct.

The system facilitates the study of combustion processes across a broad spectrum of parameters. Its most significant advantage is its excellent measurement capabilities, including the flexible installation of various types of sensors, which is difficult and sometimes impossible in industrial facilities.

The provision of air for afterburning to the combustion chamber is facilitated by three OFA (OverFire Air) nozzles, each with independently adjustable airflow and temperature.

The test bench is equipped with a control and measurement system that allows for the visualization and recording of numerous operating parameters of the bench, including medium flow rates, temperatures, and pressures in various parts of the installation, as well as the composition of exhaust gases.

Research has indicated that the potential for unstable combustion may be attributed to optical parameters, including flame surface area, contour length, and flame centre coordinates, in addition to higher air excess coefficients, irrespective

of thermal power. For a greater proportion of biomass, there was evidence of sharp changes in the parameters under discussion. This indicates that combustion is unstable [4].

The methodology employed to ascertain the flame area exerts a direct influence on the values obtained for the quantitative parameters of the flame area and its contour length. The installation of the camera perpendicular to the burner axis facilitates the assessment of crucial information pertaining to the combustion process. This encompasses the distance between the burner and the flame ignition point, as well as the angle of flame propagation. In industrial practice, it is challenging to install the camera in close proximity to the burner of full-scale power boilers. This is due to the fact that doing so can cause interference in the boiler body. Consequently, an alternative camera configuration was subjected to testing.

The co-firing process provides reliable adaptive control using optical signals. The capacity to evaluate the combustion quality is imperative for the effective functioning of the boiler. The combustion flow in the layers has been demonstrated to affect the rate of chemical reactions, the efficiency of heat transfer, flame stability, and the formation of NO_x and CO. The type of burner, fuel type, and control method are pivotal factors influencing the formation of combustion aerodynamics [8].

The most prevalent method of reducing NO_x emissions is to modify the organization of the co-combustion process. Nevertheless, this has unfavorable ramifications for the operation of the boiler. The consequences of this are an increase in unburned fuel losses, increased CO emissions, increased slagging, evaporator corrosion, and flame instability [9].

It is challenging to achieve the required level of NO_x reduction, given that these phenomena are undesirable and even dangerous for the boiler. The introduction of an appropriate monitoring and control system has the potential to address this issue. The implementation of advanced combustion control systems necessitates the introduction of additional design modifications and signals, manifesting as distinct air flows directed towards individual burners, OFA nozzles, and mill load, or supplementary signals from flue gas analyzers, including NO_x, CO, and SO₂. It is evident that the quantity of NO_x emissions in a coal-fired boiler is contingent on the amount of excess air during combustion. Consequently, it would be advantageous to regulate the combustion process within a single burner.

The combustion process occurring in chemical reactions and physical processes can be reflected by the radiation emitted by the flame. In the current state of technology, the provision of immediate and spatially selective additional information about the current combustion process can only be achieved non-invasively using optical or acoustic diagnostic methods. It is possible to include the determination of the air-fuel ratio, the amount of heat released, and the temperature in the flame spectrum range in visible radiation. An image-based approach appears to be of particular significance, given that the visible position of the flame is the result of a dynamic balance between the local flame propagation speed and the speed of the incoming fuel mixture. It is hypothesized that changes in the position of the flame front may serve as an indicator of this inevitable deformation occurring under certain conditions [10].

A potential issue with complex control systems, such as combustion processes, is the complex (and therefore incomplete) measurement of physical and chemical variables. In the proposed solution, the classical approach is supplemented with information about the flame based on selected parameters of the image recorded by a high-speed camera.

The analysis revealed a clear relationship between the parameters describing changes in the flame and the temperature of the exhaust gases in the chamber or the airflow rate in the secondary coefficient. Consequently, in circumstances where temperature fluctuations are gradual and of a neutral nature, it becomes feasible to employ fast image control synthesis (essentially a parameter or group of image parameters).

The primary air is principally utilized for feeding coal dust into the burner nozzle, while the secondary air is employed for control purposes. The input parameters, including the coal-biomass mixture and air flows, were subjected to multiple alterations during the course of the tests, thereby generating a variety of combustion conditions.

In the absence of complete knowledge of the control object or its rapid alterations in behavior, adaptive control appears to be a rational approach. A nonlinear autoregressive network with exogenous inputs (NARX) is defined as a recurrent dynamic network with feedback loops spanning several layers of the network. The NARX model is predicated on the linear ARX model, which is a widely utilized framework in time series modeling.

The non-standard architecture employed for the purposes of further analysis is known as Model Reference Adaptive Control (MRAC). The reference control architecture is comprised of two subnets. One subnet functions as a model of the controlled object, with the other subnet serving as the controller [3, 11].

The trained NARX model can be used to create an MRAC system and integrate it into the system controller structure. The necessity for the incorporation of ring connections is apparent in this context. To ensure the closed MRAC system responds similarly to the reference model (used to generate data), the weights from the trained installation model network must be correctly positioned within the MRAC system. Subsequently, to obtain an initial input signal of zero, it was necessary to set the output weights of the controller network to zero. The training of the MRAC system was found to require significantly more time than the training of the NARX plant model. This discrepancy can be attributed to the recurrent nature of the MRAC system, which necessitated the implementation of dynamic backpropagation. After training the network, its efficacy was evaluated by introducing test data into the MRAC network.

Figure 10 shows the system's response to the input setpoint in both cases: with classical measurements (a) and after applying the contour length vector for the flame descriptor (b).

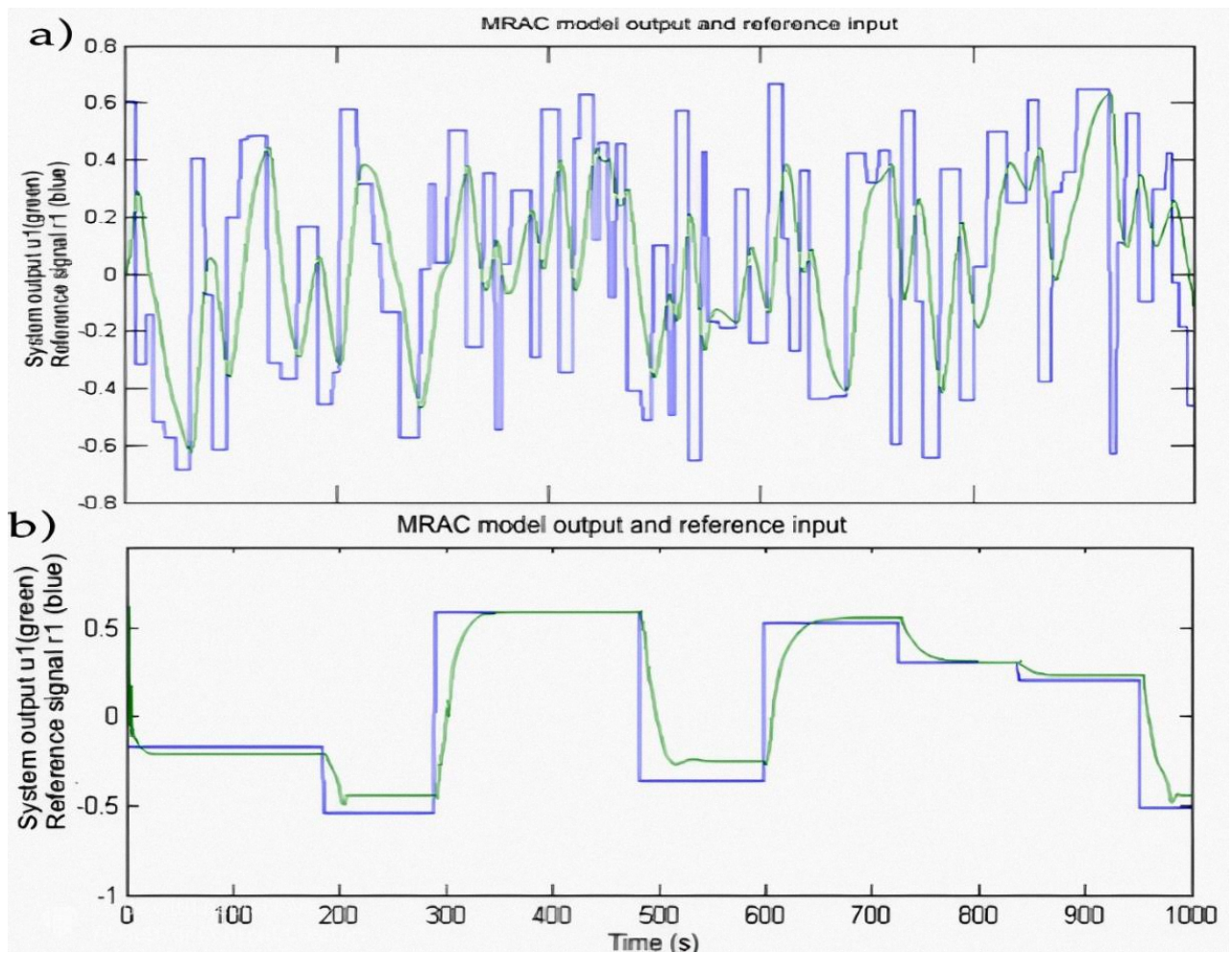


Figure 10.

Response of the dust boiler control system using (a) input data vector (b) input data extended with optical information.

As demonstrated in Figure 10, the simulation results indicate that the model output follows the reference input with a correctly damped response, even in instances where the input sequence does not correspond to the input sequence in the training data. whilst the steady-state response is not ideal at every stage, improvements can be made through the use of a larger training set and potentially more hidden neurons. it is evident from the findings of the study that the control signals are constrained, and that sudden alterations in system parameters necessitate corresponding changes in the amplitudes of the command laws and outputs of the controlled system.

As previously stated, the imposition of restrictions can serve as a mechanism to ensure reliability. The control system under scrutiny was subjected to a simulation of a sudden load surge.

This test reproduces a critical situation that occurs when there is an unexpected change in the strength and quantity of NOx radicals. The results are shown in Figure 11.

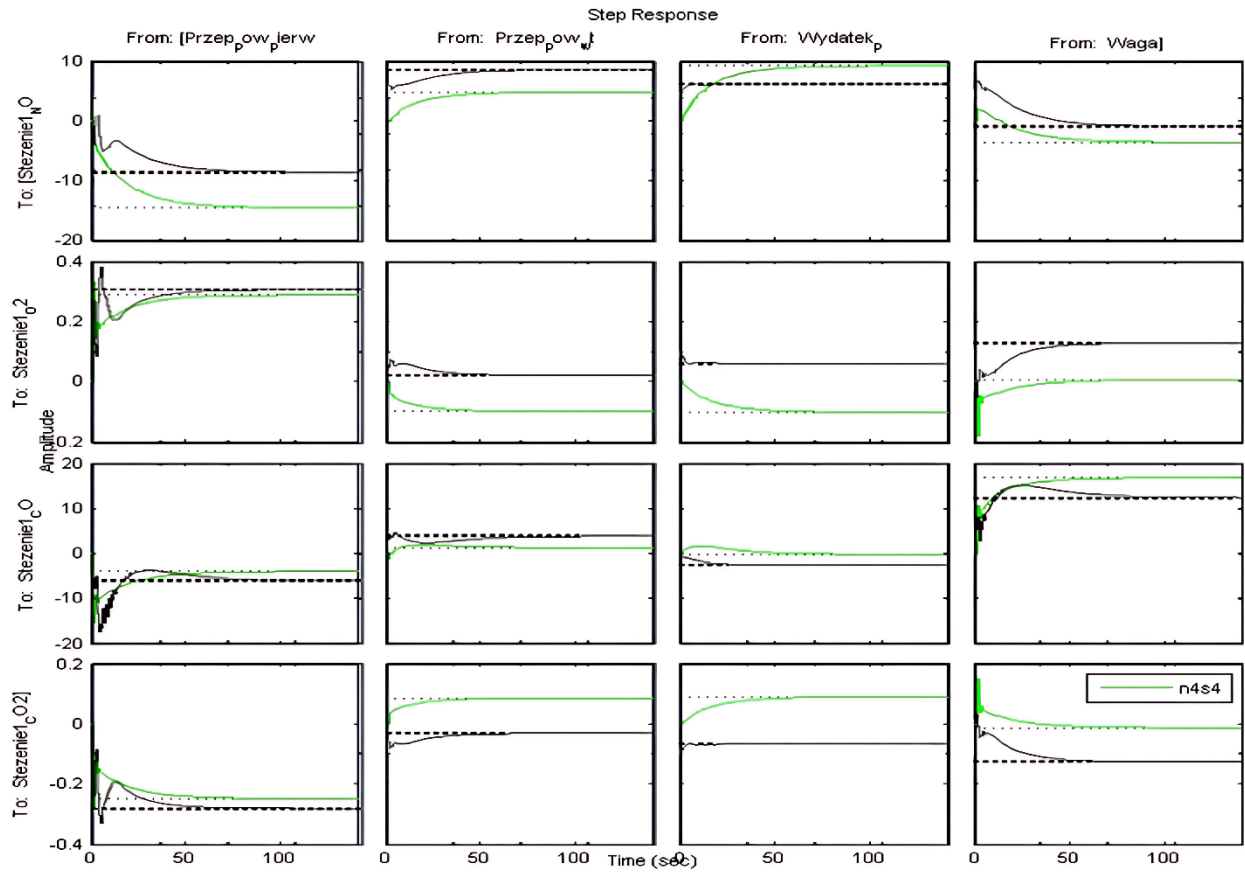


Figure 11.

The response of the MIMO controller to a sudden change in power load, taking into account the ratio of NOx and CO concentrations and the temperature of the exhaust gases in the combustion chamber.

The constraints are satisfied because the algorithm has checked all possible values of uncertainty. The flame area is widely used as one of the primary indicators of the combustion process. Consequently, it can be deduced from a series of images and utilized with expeditious access to information (ideally in real-time systems).

In the most elementary instance, burner diagnostics entails the identification of the presence or absence of a flame. In low-emission swirl burners, under normal operating conditions, the flame ignites on the burner ring, and this position stabilizes [12]. However, under certain operating conditions of the burner, such as when operating at low power or with very wet fuel, the flame may detach from the burner ring. This can negatively affect the combustion process and may also be misinterpreted by existing sensors as the absence of a flame (Figure 12).

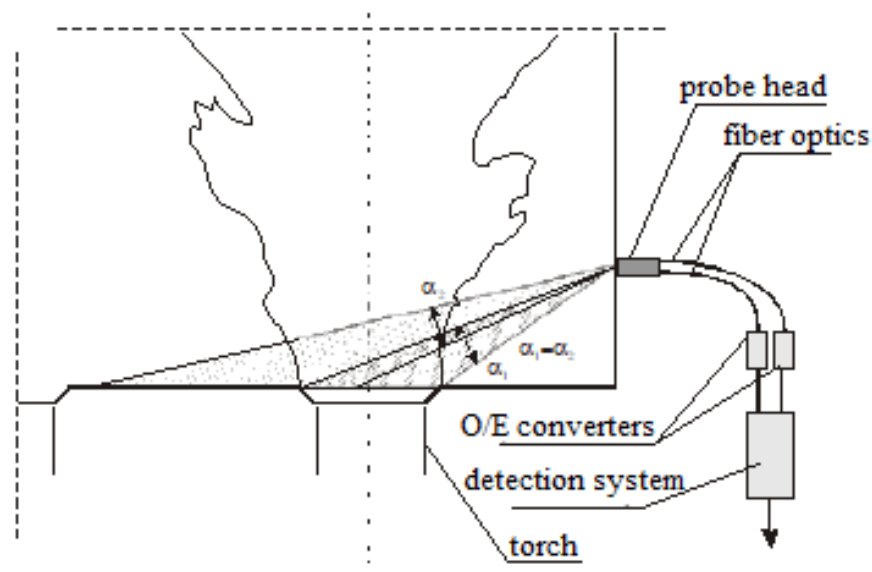


Figure 12.

Detection of flame separation from the burner ring.

A fibre optic sensor, capable of detecting flame separation from the rim of a low-emission burner, is placed on the wall of the power boiler at a perpendicular angle to the wall on which the low-emission vortex burners are mounted. The sensor head contains two fibre optic cables. The primary component is installed with the intention of ensuring that the receiving cone, which is characterized by a fibre optic reception angle limitation (α_1), encompasses the burner rim with a marginal excess. The second fibre optic cable exhibits a reception angle limitation (α_2) that is congruent with the first and is oriented towards the interior of the combustion chamber, thereby ensuring that the reception angles share a common part [13]. It is evident that the receiving cone of the second fibre optic cable does not extend to the adjacent burners. The axes of symmetry of the burner and both fibre optic cables are found to lie in the same plane. The fibre optic cables are connected to optoelectronic converters, where the optical signal from the fibre optic cables is converted into electrical signals containing information about changes in the intensity of the flame base glow. Subsequently, the variable component is extracted from both electrical signals. The absence of the variable component in the signal from the first fibre optic cable, in conjunction with a variable signal from the second cable, indicates that the flame has become detached from the burner crown. The condition is detected by an electronic detector with a standard electrical output [14].

3. Results of the Study

During the testing phase, the error in the neural network estimation of nitrogen oxide emissions, based on optical measurements, did not exceed 10% for any of the samples, with an average value of approximately 3%. The optical-neural network system for estimating combustion parameters was used in the control system for stabilizing nitrogen oxide emissions from a single burner.

As illustrated in Figure 13, the results of the simulation tests demonstrate a comparison of the response of the control system operating on the basis of a signal from a gas analyzer (thin line) and on the basis of signals from an optical probe (thick line). For analytical reasons, the output signals were synchronized in such a way as to eliminate the delay introduced by the gas analyzer.

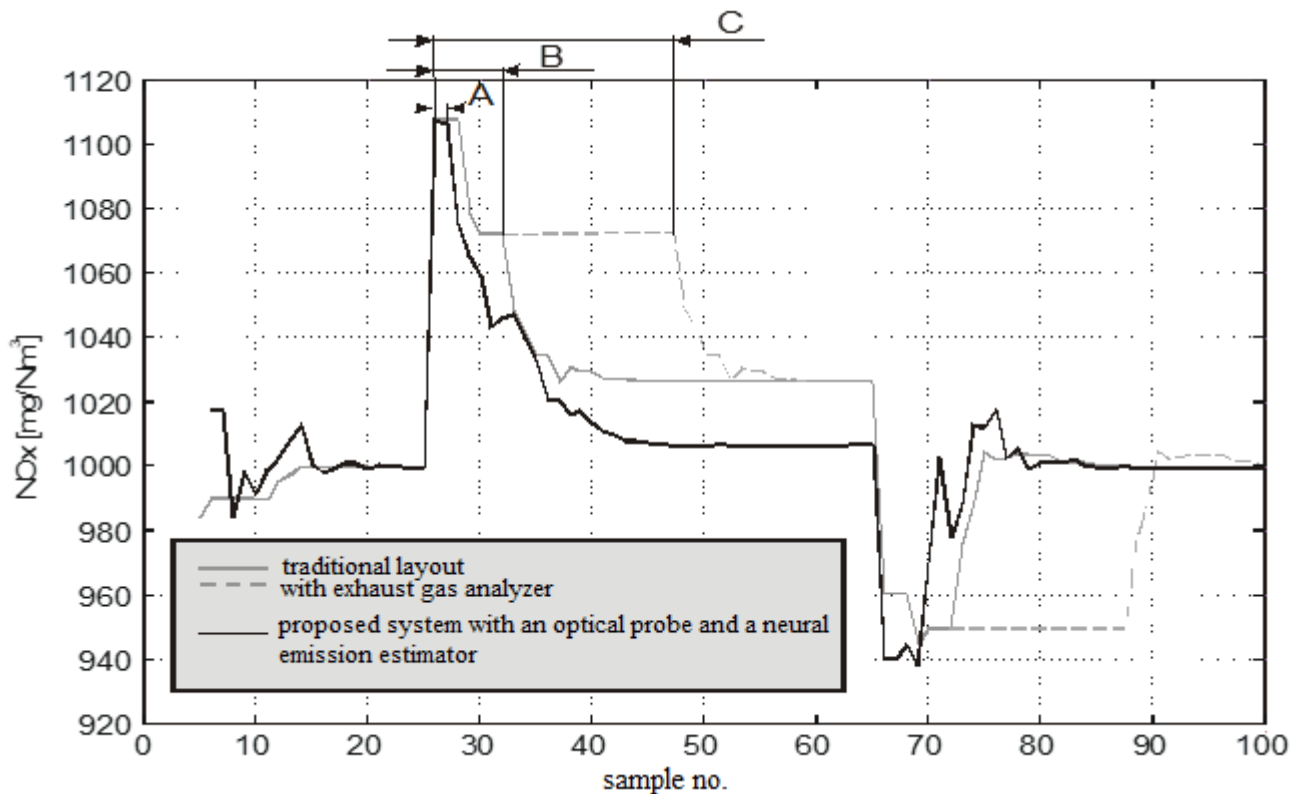


Figure 13.

Comparison of the object's response to NPC using different methods of obtaining feedback on the amount of nitrogen oxide emissions.

When appropriate regulator parameter values are employed in a system equipped with a fibre optic probe and a neural emission estimator, a response settling time of approximately 20 sampling periods can be achieved. This value is comparable to that achievable in a system with a gas analyser [15]. The advantage of this solution is that it allows for the incorporation of a single burner within the control loop. Additionally, it facilitates a considerably reduced system response time to disturbances, that is to say, a more rapid return to the full disturbance value at the output. Consequently, this results in a diminished emission of pollutants. The control system with an optical probe (designated "A" in the schematic) exhibits a delay time that does not exceed two sampling periods. In the case of a traditional solution (designated "B" in the figure), the time delay is determined by the measuring system's latency. In the case of large facilities, such as power boilers at power plants, the delay can be as long as several hundred seconds, depending on the analyzers used [4]. In such cases, a system equipped with a gas analyzer will be unable to detect increased emissions during the delay. This will result in

increased emissions persisting for a significant duration, as demonstrated in Figure 13 by the dotted line. The variable "C" denotes the delay time between the occurrence of increased emissions and their detection by gas analyzers. Laboratory tests conducted for a gas burner have shown that an optical combustion parameter estimator combined with a fuzzy controller has good adaptability to changing operating conditions and fuel types, keeping NO_x and CO emissions below the required levels despite the considerable complexity of the task at hand. Preliminary findings in conditions of variable fuel composition demonstrate the capacity to estimate combustion parameters through the measurement of optical flame parameters, obviating the necessity for knowledge of the composition of the combusted gases.

Determining the parameters of the combustion process model for a single low-emission burner is an important element in the synthesis of a superior control system that will take into account diagnostic information from the optical flame monitoring system. The experiments encompass the stabilization of the operating point of the laboratory stand at varying power levels, diverse fuel types (including coal and biomass), and three interchangeable types of low-emission burners (with different blade angles) [16]. The measurement of process parameters is conducted at a frequency of 1 Hz. The recorded values include multi-point measurements of exhaust gas concentrations (NO_x, O₂, CO, CO₂), measurements of temperatures, pressures, and flows, as well as fan control levels. Optical measurements are performed at a frequency of 1 kHz.

The initial stage of work will include analysis of selected, registered input and output values. For the synthesis of multidimensional (MIMO) models, input signal vectors were determined that quantitatively describe the secondary air flow rate and fuel consumption, and output signal vectors were determined that describe the concentrations of NO_x, CO, and the temperature of the exhaust gases in the chamber, recorded at the first measurement point [17].

The data was divided into training and test sets using a 70% and 30% split, respectively. Using the System Identification Toolbox, the parameters for the parametric models were identified within the state space of the data using the system:

$$\begin{cases} (t + Ts) = Ax(t) + Bu(t) + Ke(t) \\ y(t) = Cx(t) + Du(t) + e(t) \end{cases}, \quad (1)$$

at specific operating points (three heat output values, temperature stabilization, uniform fuel). The choice of model order was empirical. In most cases, it took a value from the range <3, 11>. The fitting results (in MSE, expressed as a percentage) are presented in Table 2.

Table 2.

Mean square error values for the identification of individual parametric models of the first and second degree.

Test set	Models 1					
	P1		P2		P3	
	D1M1_4s11	D1M1_4s6	D2M1_4s6	D2M1_4s5	D3M1_4s3	D3M1_4s4
D1	64.77	59.89	58.51	57.98	56.92	58.65
D2	47.28	57.48	60.25	59.42	55.51	56.49
D3	62.65	64.84	63.41	64.12	66.81	70.25
Test set	Models 2					
	P1		P2		P3	
	D1M2_4s10	D1M2_4s3	D2M2_4s4	D2M2_4s10	D3M2_4s10	D3M2_4s6
D1	64.58	62.62	61.67	59.77	54.33	54.96
D2	67.23	66.22	71.14	73.33	59.12	58.65
D3	53.06	55.39	53.74	53.14	54.47	52.35

The complex object under scrutiny is regarded as a system characterized by a sequential structure. Consequently, the output data of the first-level models serve as the input data for the second-level models (designated in Table 2 as Models 2), which delineates the relationships between NO_x and CO concentrations, exhaust gas temperature in the chamber, and analogous values at the corresponding measurement point [2, 18].

Figure 14 shows the step responses of P2 models to a unit step excitation.

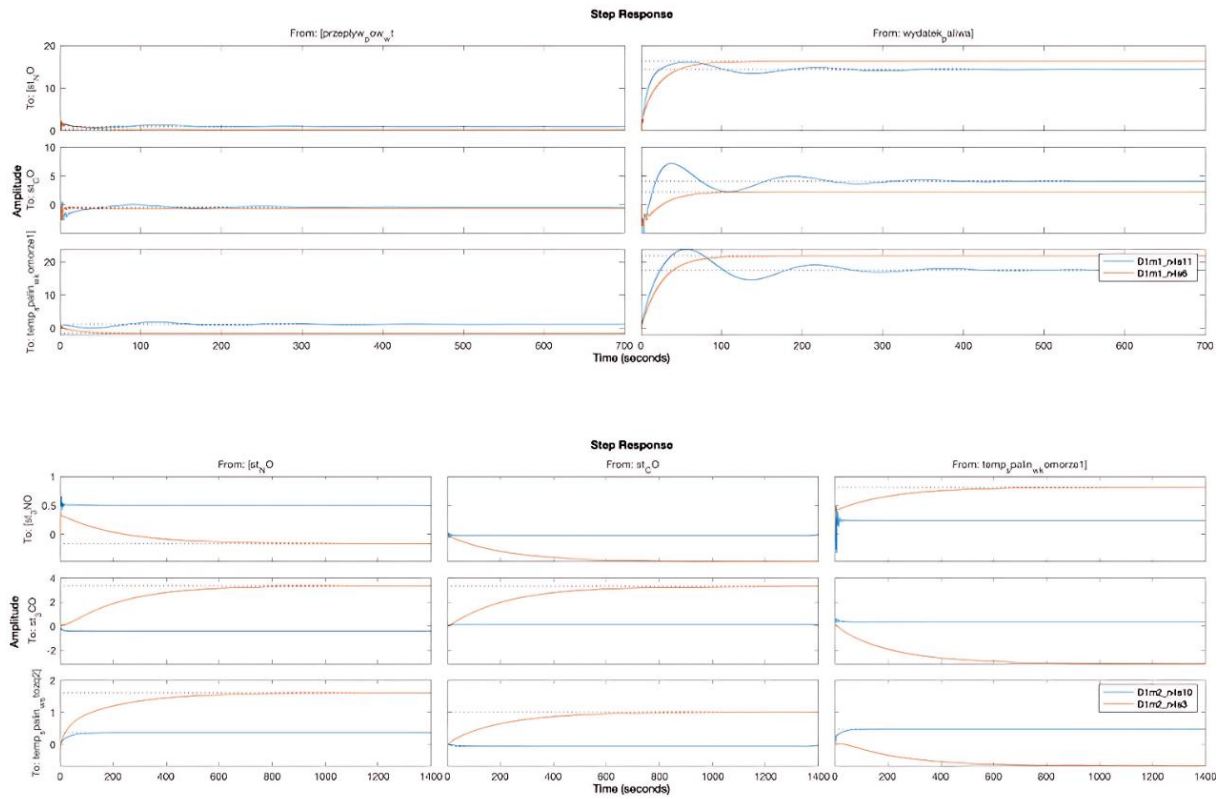


Figure 14.
Response characteristics of P1 models to single excitation.

Figure 15 shows the step responses of P2 models to a unit step excitation.

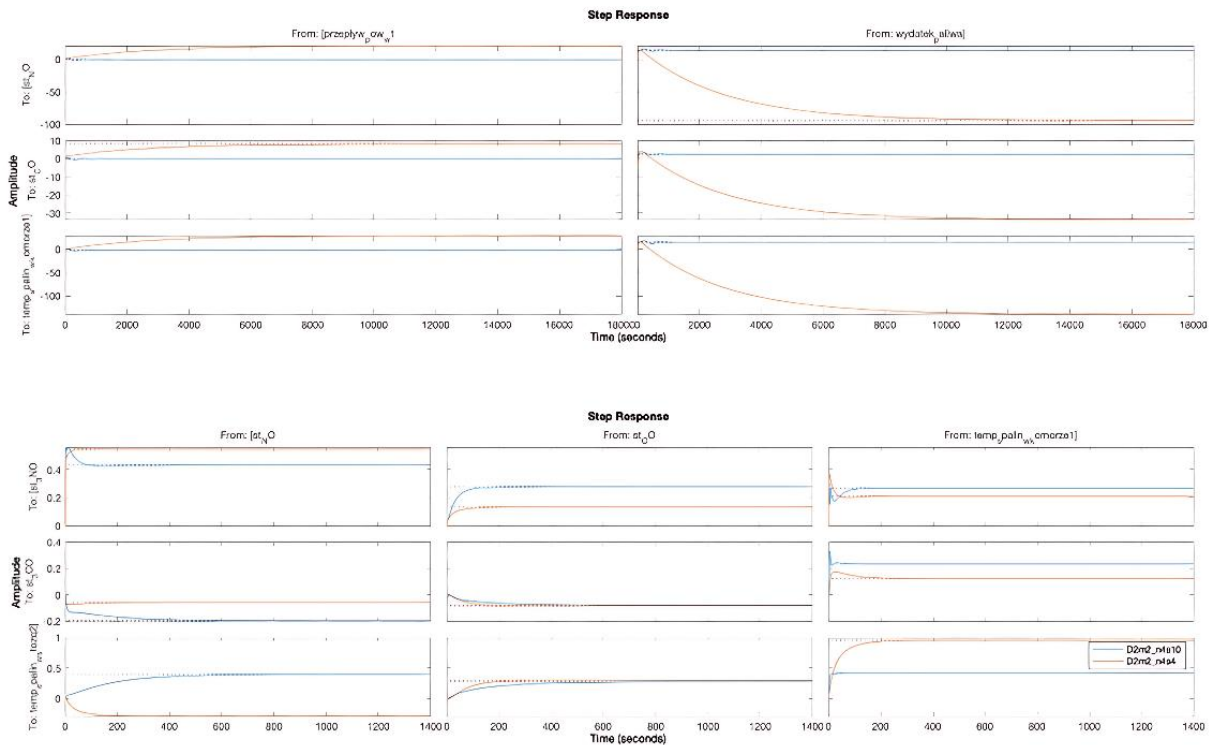


Figure 15.
Response characteristics of P2 models to single excitation.

Figure 16 shows the step responses of P3 models to a single step excitation.

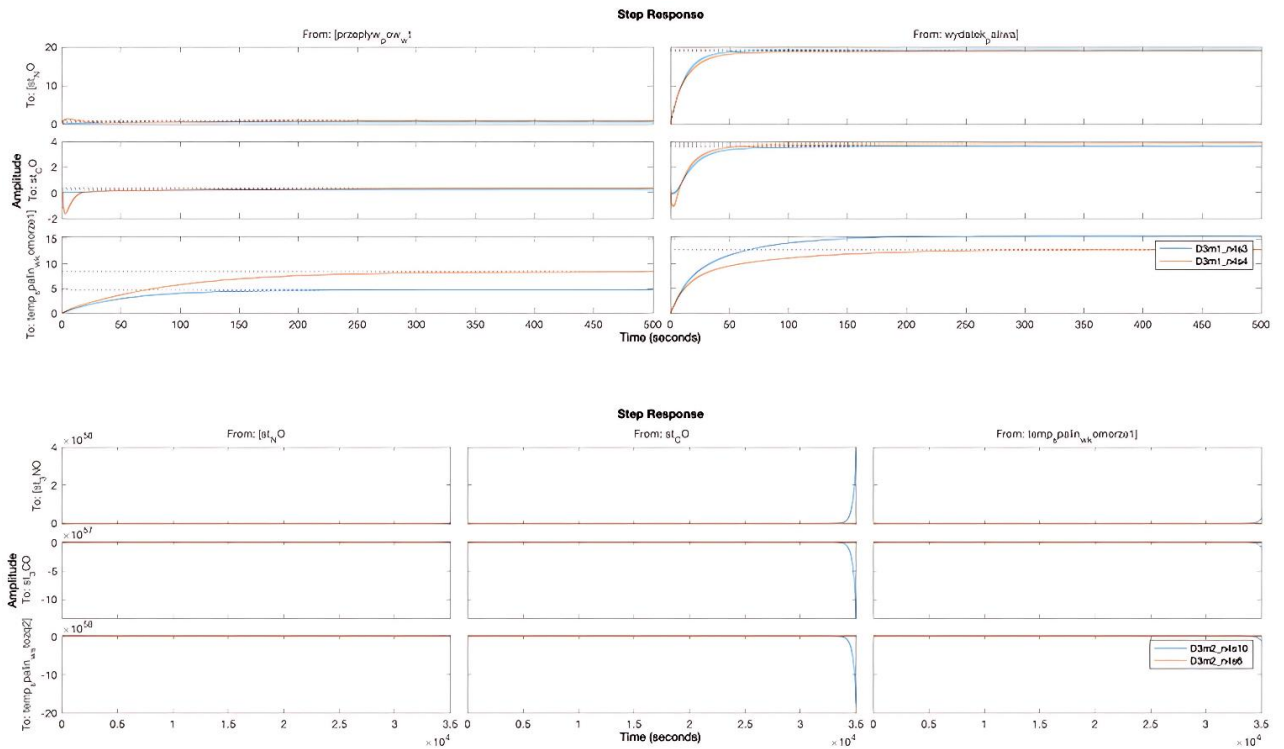


Figure 16.
Response characteristics of P3 models to single excitation.

Models with an accuracy of 60% were selected for further analysis.

Verification of the simulation model. To verify the reliability of the models obtained, an MPC (Model Predictive Control) controller was developed using Matlab/Simulink platform tools (Figure 17):

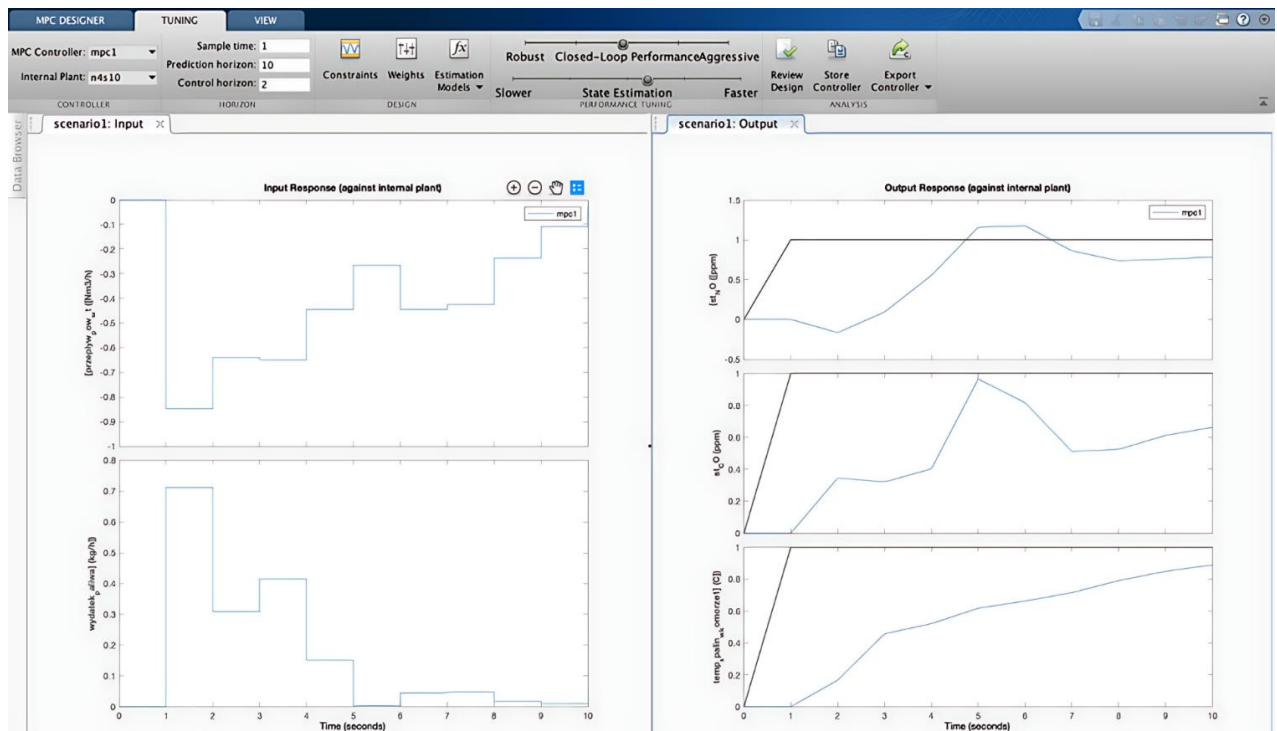


Figure 17.
Design and configuration of the MPC controller.

It allows you to set limits on output and control signals, disturbance signals, and establish forecasting and control horizons. This makes it possible to test models within the context of regulatory constraints (e.g., NOx emissions) [19].

The presented Simulink diagram with the developed process control system model considers the possibility of switching between manual and automatic modes of operation (Figure 18).

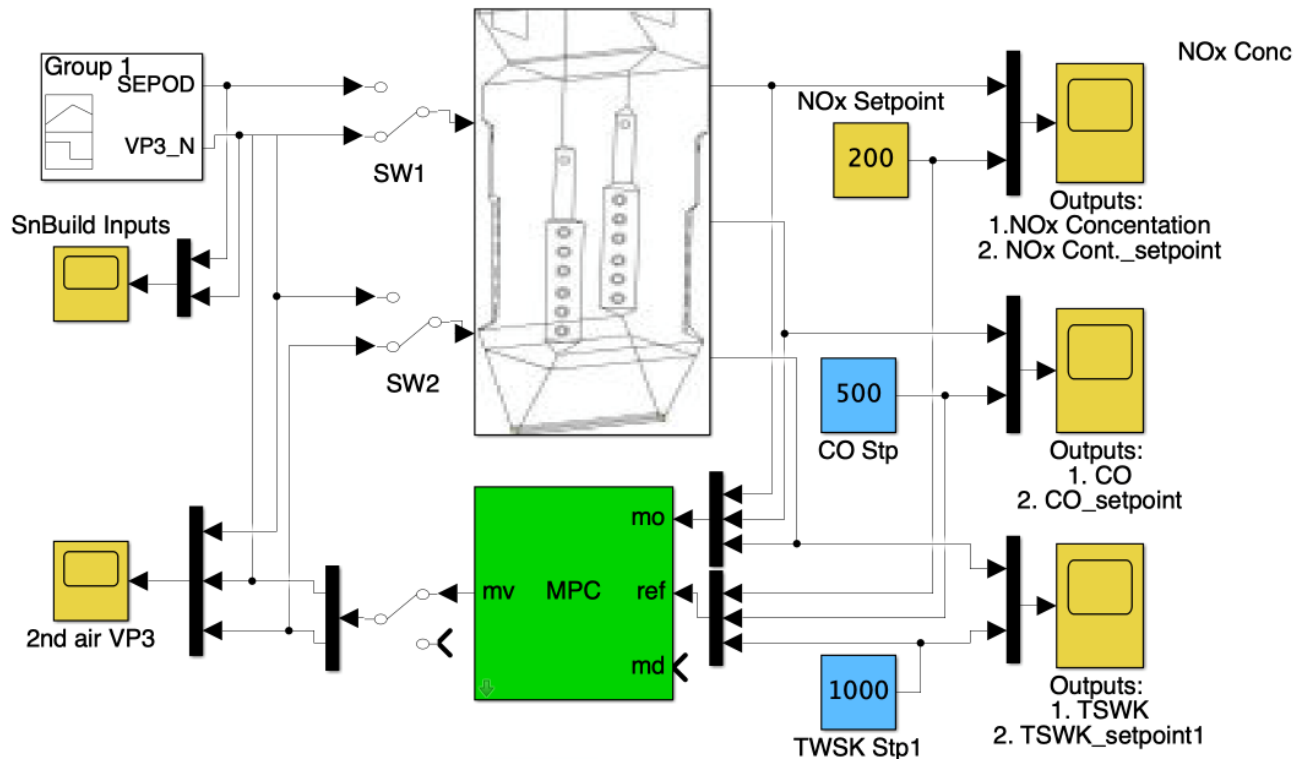


Figure 18.
Simulink diagram of the control system under test.

The MPC controller used in the system minimizes the differences between the values of the controlled variables $y(k + p|k)$ predicted at time k for the future time $k+p$ (i.e., the future values at time $k+p$ are determined based on the values at time k) and the set values for these outputs $y_{zad}(k+p|k)$ at the forecast horizon N ($p=1,2,\dots,N$). Minimization of differences is understood in terms of a specific quality criterion. At the next moment $k+1$, a new measurement of the object's output signal is made, and the entire procedure is repeated with the same forecast horizon N . Thus, the principle of a sliding horizon (also called repetition control) is applied. In the forecasting algorithm, it is assumed that after the so-called control horizon N_u (usually $N_u < N$), the increment of the control signal is equal to 0.

The criterion function is generally defined by the ratio [2, 20]:

$$J(k) = \sum_{p=N_1}^N \|y_{zad}(k+p|k) - y(k+p|k)\|_{\Psi(p)}^2 + \sum_{p=0}^u \|\Delta u(k+p|k)\|_{\Lambda(p)}^2, \quad (2)$$

where: $\Delta u(k+p|k)$ – control increment vector, $\Psi(p) \geq 0$ – matrix of weight coefficients of error vector components predicted at time $k+p$ (most often diagonal) and $\Lambda(p) \geq 0$ – matrix, where: $y_{zad}(k+p|k)$ – vector of a specified value, $y(k+p|k)$ – vector of controlled variables, weight coefficients, components of the control increment vector, predicted at the current moment $k+p$. When $\Lambda(p) = \lambda I$ to, $\lambda \geq 0$ determines the importance of damping control variability in relation to control error reduction.

Within the scope of the tests conducted, considering the NOx emission limits (300 ppm), the best NRMSE results were obtained for the low-emission models of the first (D1M1_4s6) and third (D3M1_4s3) burners (Figure 19) [2, 21].

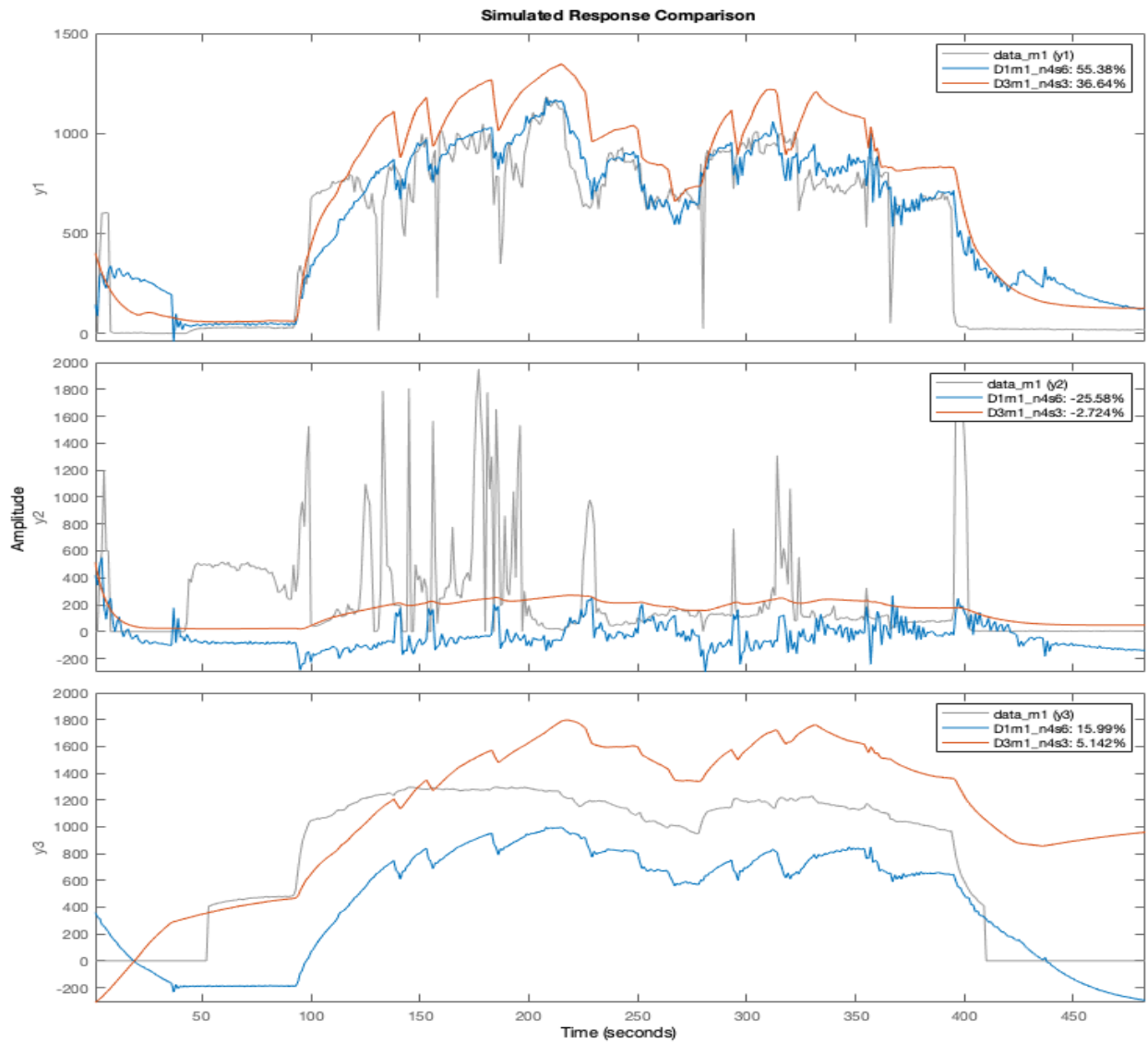


Figure 19.
Comparison of P1 model responses for combustion test data.

In the case of P2 models, compliance with emission limits was achieved with fluctuations (D2M1_4s5), while in the case of (D2M1_4s6), it ended in failure. The sequential configuration yielded the best results in combination with model structures (D2M2_4s4 and D2M2_4s10) (Figure 20).

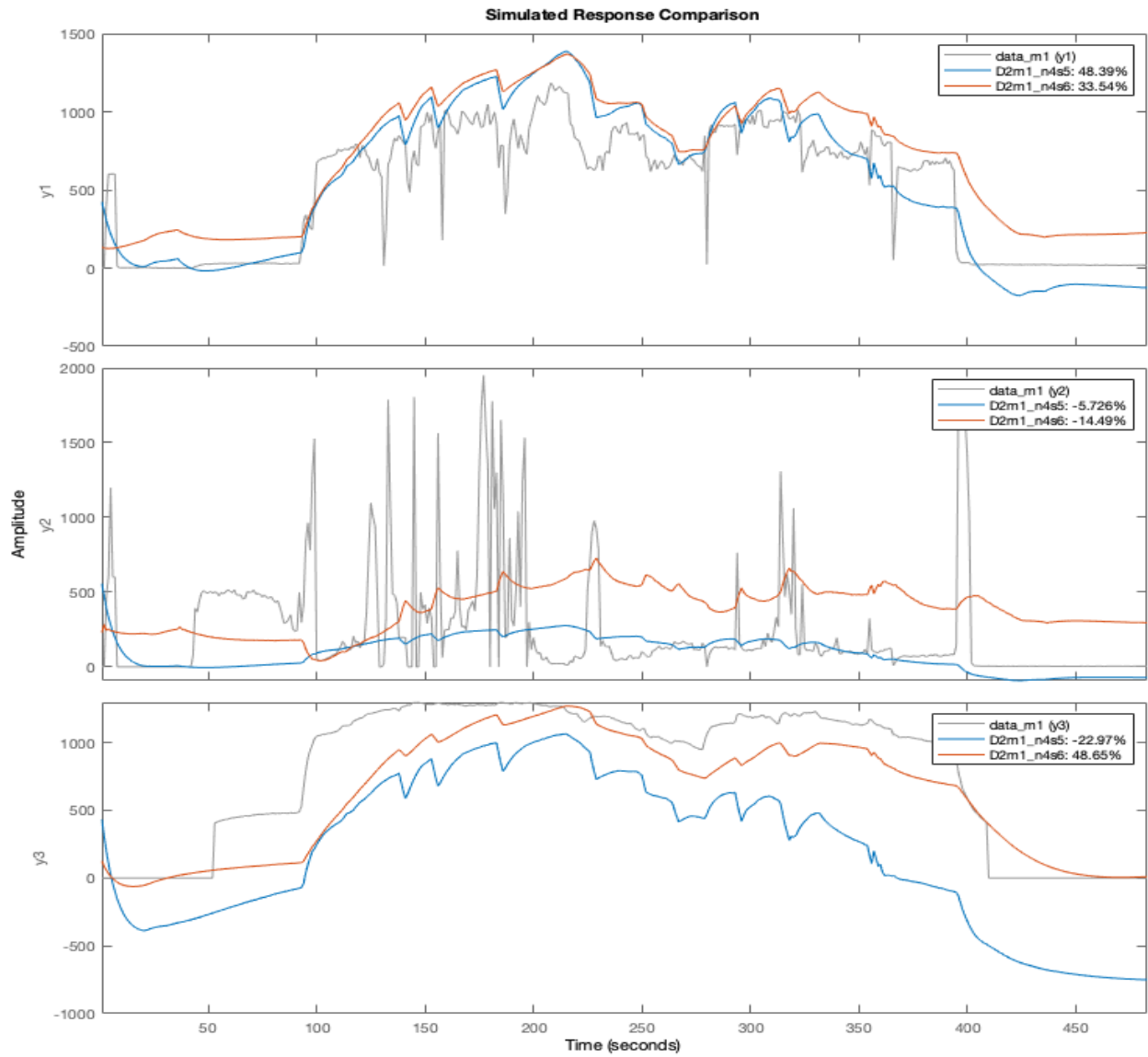


Figure 20.
Comparison of PI model responses for combustion test data.

It is evident from the presented characteristics of the response to test input signals of the real process that there are relatively large differences between individual models [22].

Empirical Wavelet Transform (EWT) is a novel signal processing method that constructs wavelets based on the spectrum of the analyzed signal. EWT can be implemented as follows [4, 23]:

- Applying the Fourier transform of the analyzed signal, divided into N adjacent segments according to Algorithm 1;
- Empirical scaling of functions and the determination of empirical wavelets using algorithms based on formulas (1) and (2), respectively.
- Calculating the approximation and detail coefficients according to dependencies (3) and (4).

$$\hat{\Phi}_n(\omega) = \begin{cases} 1 & \text{dla } |\omega| \leq (1 - \gamma)\omega_n \\ \cos \left[\frac{\pi}{2} \beta \left(\frac{1}{2\gamma\omega_n} (|\omega| - (1 - \gamma)\omega_n) \right) \right] & \text{dla } (1 - \gamma)\omega_n \leq |\omega| - (1 - \gamma)\omega_n, \end{cases} \quad (1)$$

$$\hat{\Psi}_n(\omega) = \begin{cases} 0 & \text{otherwise} \\ 1 & \text{if } (1 + \gamma)\omega_n \leq |\omega| \leq (1 - \gamma)\omega_{n+1} \\ \cos \left[\frac{\pi}{2} \beta \left(\frac{1}{2\gamma\omega_{n+1}} (|\omega| - (1 - \gamma)\omega_{n+1}) \right) \right] & \text{if } (1 - \gamma)\omega_{n+1} \leq |\omega| \leq (1 + \gamma)\omega_{n+1} \\ \sin \left[\frac{\pi}{2} \beta \left(\frac{1}{2\gamma\omega_n} (|\omega| - (1 - \gamma)\omega_n) \right) \right] & \text{if } (1 - \gamma)\omega_n \leq |\omega| \leq (1 + \gamma)\omega_n \\ 0 & \text{otherwise} \end{cases}, \quad (2)$$

$$w_f^\varepsilon(0, t) = \langle f, \phi_1 \rangle = \int f(\tau) \overline{\phi_1(\tau - 1)} d\tau = (\hat{f}(\omega) \overline{\phi_1(\omega)})^\wedge, \quad (3)$$

$$w_f^\varepsilon(n, t) = \langle f, \varphi_n \rangle = \int f(\tau) \overline{\varphi_n(\tau - 1)} d\tau = (\hat{f}(\omega) \overline{\varphi_n(\omega)})^\wedge, \quad (4)$$

In addition, there are some limitations to maintaining the effectiveness of this algorithm. For example, the coefficient γ in Equations 1 and 2 is limited to a small value $\gamma < \min_n \frac{(\omega_{n+1} - \omega_n)}{(\omega_{n+1} + \omega_n)}$ to ensure the empirical scaling function and that the empirical wavelets form a narrow frame of the $L^2(R)$ space. In turn, the coefficient $\beta(x)$ is defined as $\beta(x) = x^4(35 - 74x + 73x^2 - 18x^3)$. The inverse empirical wavelet transform can be calculated based on equation (5):

$$f(t) = w_f^\varepsilon(0, t) * \phi_1(0, t) + \sum_{n=1}^N w_f^\varepsilon(n, t) * \psi_n(t) = (\hat{w}_f^\varepsilon(0, \omega) \hat{\phi}_1(\omega) + \sum_{n=1}^N \hat{w}_f^\varepsilon(n, \omega) \hat{\psi}_n(\omega)) \quad (5)$$

4. Conclusions

In this study, the inverse empirical wavelet transform is utilized to rectify the emissions of the forecast series. To this end, the spectral segments of the trained series are used as estimates of the combined series, thereby establishing a linkage between the trained series and the forecast series [24].

The figure presents a petal diagram for specific indicators of modelling effectiveness (Figure 21). In order to ensure an effective comparison of the proposed models, a number of performance indicators were considered, including mean absolute error (MAE), mean absolute percentage error (MAPE), standard deviation of error (SDE), and root mean square error (RMSE).

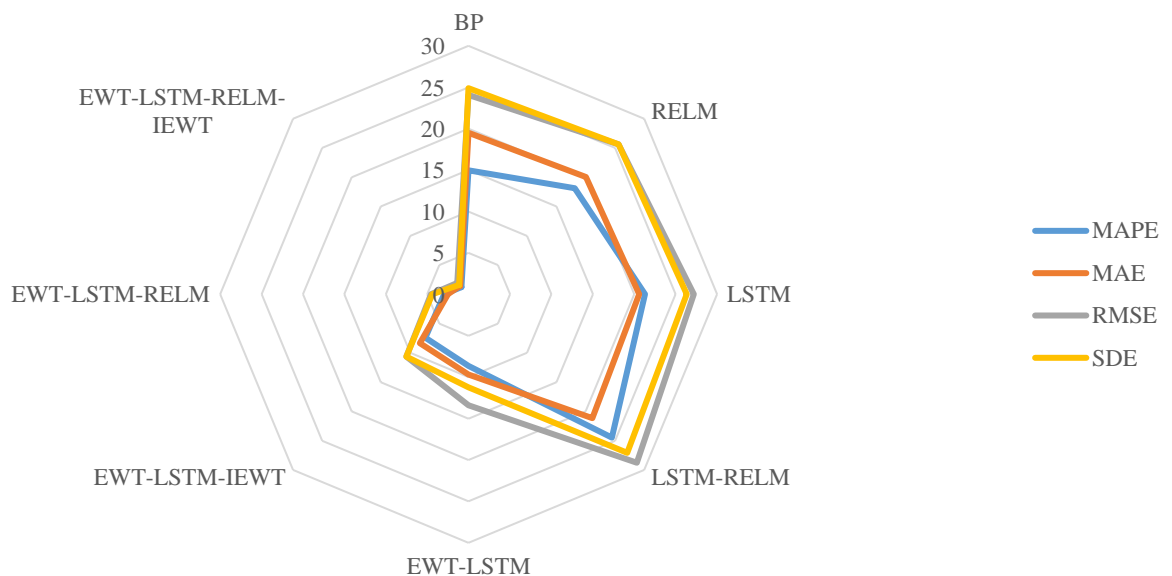


Figure 21.
Petal chart of model accuracy indicators.

The study considered direct forecasting with a five-step horizon. According to the analysis results, the best results in modeling the time series of the combustion process were obtained using the hybrid EWT-LSTM-RELM-IEWT method.

The least attractive model in this comparison was the single backpropagation (BP) model. The regularized extreme learning machine (RELM), both alone and in combination with the LSTM model, provided average RMSE and SDE values that were almost an order of magnitude higher.

The IEWT algorithm was used to reconstruct complex sublayers and obtain final prediction results. Despite the relatively high computational complexity, model hybridization appears to be the appropriate approach for predicting complex processes.

References

- [1] L. N. Yesmakhanova, *Controlling the combustion of pulverized coal using advanced technologies [Text]: Monograph / L.N. Yesmakhanova* Taraz: Taraz University, 2019.
- [2] L. Yesmakhanova et al., "Simulating the coal dust combustion process with the use of the real process parameters," *ARP Journal of Engineering and Applied Sciences*, vol. 16, no. 22, pp. 2395-2407, 2021.
- [3] W. Wójcik, J. Ballester, A. Kotyra, A. Sanz, and R. Hernández, "Neural methods of interpretation of data obtained from optical sensor for flame monitoring in optical fibers: Applications," in *Proceedings of SPIE, Volume 5952, Optical Fibers: Applications (pp. 59521L-1-59521L-6)*. Bellingham, WA: SPIE, 2005. <https://doi.org/10.1117/12.622953>
- [4] W. Wójcik and A. Smolarz, "Stabilization of NOx emissions from a single pulverized coal burner using NPC and neural combustion parameter estimation method," *Pomiary Automatyka Kontrola*, vol. 53, no. 11, pp. 20-23, 2007.

- [5] W. Wójcik, A. Kotyra, A. Smolarz, and B. Pilek, "Controlling combustion process in power boiler by genetic algorithm and neural network," in *Proceedings of SPIE, Photonics Applications in Industry and Research III*, Vol. 5775 (pp. 348–353). Bellingham, WA: SPIE, 2005. <https://doi.org/10.1117/12.610685>
- [6] A. S. Askarova, "Three-dimensional modeling of the processes of formation of harmful substances during the combustion of low-grade coals in combustion chambers [Text] / A.S. Askarova, S.A. Bolegenova, V.Yu. Maximov," *Bulletin of the National Academy of Sciences of the Republic of Kazakhstan*, vol. 6, pp. 15-18, 2010.
- [7] A. S. Askarova, S. A. Bolegenova, V. Y. Maximov, and A. Bekmukhamet, "Effect of the computational grid size on the results of computer modeling of heat and mass transfer processes in combustion chambers," presented at the 18th All-Russian Scientific Conference of Young Scientists (VNKSF-18), Krasnoyarsk, Russia. Materials, Publishing House of Russia, 2012.
- [8] O. N. Novikov, "Energy-ecological optimization of fuel combustion in boilers and furnaces by regulating the fuel-air ratio," *Industrial Energy*, p. 288, 2000.
- [9] A. E. Bryson Jr, W. F. Denham, and S. E. Dreyfus, "Optimal programming problems with inequality constraints," *AIAA Journal*, vol. 1, no. 11, pp. 2544-2550, 1963. <https://doi.org/10.2514/3.2107>
- [10] S. Broomhead and D. Lowe, "Multivariable functional interpolation and adaptive network," *Complex Systems*, vol. 2, pp. 321-323, 1988.
- [11] K. Jaroszewski, "Diagnostic system of the flue gas purification installation of the power plant using artificial euronetic networks," Ph.D. Thesis, Szczecin University of Technology, 2007.
- [12] I. G. Chyzh *et al.*, "Energy resolution of dual-channel opto-electronic surveillance system," in *Proceedings of the Photonics Applications in Astronomy, Communications, Industry, and High-Energy Physics Experiments, Wilga, Poland, 31 August–2 September 2020 (Vol. 11581, Paper 115810K)*. Bellingham, WA: SPIE, 2020.
- [13] W. Wójcik and A. Smolarz, "Using the neural method of estimating combustion parameters to regulate the operation of a pulverized coal burner," *Pomiary Automatyka Kontrola*, vol. 51, pp. 30-33, 2005.
- [14] V. G. Kolobrodov, G. S. Tymchik, M. S. Kolobrodov, A. S. Vasyura, P. Komada, and Z. Azehsova, "The output signal of a digital optoelectronic processor," in *Proceedings of the SPIE Photonics Applications in Astronomy, Communications, Industry, and High-Energy Physics Experiments, Wilga, Poland, 2018*.
- [15] K. Tainaka *et al.*, "Measurement techniques for soot in pulverized coal combustion fields," *Journal of the Society of Powder Technology*, vol. 55, no. 5, pp. 275–281, 2018. <https://doi.org/10.4164/sptj.55.275>
- [16] F. Tian, H. Zhang, and Y. Tian, "Design and implementation of furnace temperature measurement system for power plant coal-fired boiler in acoustic method," presented at the The In MATEC Web of Conferences (Vol. 232, p. 04031). EDP Sciences, 2018.
- [17] W. Xu, Y. Yan, X. Huang, and Y. Hu, "Quantitative measurement of the stability of a pulverized coal fired flame through digital image processing and statistical analysis," *Measurement*, vol. 206, p. 112328, 2023. <https://doi.org/10.1016/j.measurement.2022.112328>
- [18] Y. Huang, X. Liu, and M. Xu, "Online measurement of soot formation distribution along time and axial in the volatile flames of coal and biomass using light scattering," *Journal of the Energy Institute*, vol. 105, pp. 33-41, 2022. <https://doi.org/10.1016/j.joei.2022.07.013>
- [19] J. Matthes *et al.*, "Camera based flame stability monitoring and control of multi-burner systems using deep learning based flame detection," *Thermal Science and Engineering Progress*, vol. 41, p. 101859, 2023. <https://doi.org/10.1016/j.tsep.2023.101859>
- [20] S. Li, T. Xu, P. Sun, Q. Zhou, H. Tan, and S. Hui, "NOx and SOx emissions of a high sulfur self-retention coal during air-staged combustion," *Fuel*, vol. 87, no. 6, pp. 723-731, 2008. <https://doi.org/10.1016/j.fuel.2007.05.043>
- [21] M. Mollo, A. Kolesnikov, and S. Makgato, "Simultaneous reduction of NOx emission and SOx emission aided by improved efficiency of a Once-Through Benson Type Coal Boiler," *Energy*, vol. 248, p. 123551, 2022. <https://doi.org/10.1016/j.energy.2022.123551>
- [22] C. Wang, Y. Liu, S. Zheng, and A. Jiang, "Optimizing combustion of coal fired boilers for reducing NOx emission using Gaussian Process," *Energy*, vol. 153, pp. 149-158, 2018. <https://doi.org/10.1016/j.energy.2018.01.003>
- [23] L.-G. Zheng, H. Zhou, K.-F. Cen, and C.-L. Wang, "A comparative study of optimization algorithms for low NOx combustion modification at a coal-fired utility boiler," *Expert Systems with Applications*, vol. 36, no. 2, Part 2, pp. 2780-2793, 2009. <https://doi.org/10.1016/j.eswa.2008.01.088>
- [24] L. Ma, Q. Fang, C. Yin, H. Wang, C. Zhang, and G. Chen, "A novel corner-fired boiler system of improved efficiency and coal flexibility and reduced NOx emissions," *Applied Energy*, vol. 238, pp. 453-465, 2019. <https://doi.org/10.1016/j.apenergy.2019.01.084>